Available online at www.sciencedirect.com
SCIENCE DIRECT®
Journal of Computational Physics 192 (2003) 695–726
JOURNAL OF COMPUTATIONAL PHYSICS
www.elsevier.com/locate/jcp

Second-order accurate kinetic schemes for the ultra-relativistic Euler equations ☆

Matthias Kunik, Shamsul Qamar *, Gerald Warnecke

Institute for Analysis and Numerics, Otto-von-Guericke University, PSF 4120, Magdeburg D-39106, Germany

Received 20 May 2003; received in revised form 31 July 2003; accepted 31 July 2003

Abstract

A second-order accurate kinetic scheme for the numerical solution of the relativistic Euler equations is presented. These equations describe the flow of a perfect fluid in terms of the particle density n, the spatial part of the four-velocity $\mathbf{u}$ and the pressure p. The kinetic scheme, is based on the well-known fact that the relativistic Euler equations are the moments of the relativistic Boltzmann equation of the kinetic theory of gases when the distribution function is a relativistic Maxwellian. The kinetic scheme consists of two phases, the convection phase (free-flight) and collision phase. The velocity distribution function at the end of the free-flight is the solution of the collisionless transport equation. The collision phase instantaneously relaxes the distribution to the local Maxwellian distribution. The fluid dynamic variables of density, velocity, and internal energy are obtained as moments of the velocity distribution function at the end of the free-flight phase. The scheme presented here is an explicit method and unconditionally stable. The conservation laws of mass, momentum and energy as well as the entropy inequality are everywhere exactly satisfied by the solution of the kinetic scheme. The scheme also satisfies positivity and L^1-stability. The scheme can be easily made into a total variation diminishing method for the distribution function through a suitable choice of the interpolation strategy. In the numerical case studies the results obtained from the first- and second-order kinetic schemes are compared with the first- and second-order upwind and central schemes. We also calculate the experimental order of convergence and numerical L^1-stability of the scheme for smooth initial data.

AMS: 65M99; 76Y05

Keywords: Relativistic Euler equations; Kinetic schemes; Second-order accuracy; Conservation laws; Hyperbolic systems; Entropy conditions; Positivity; L^1-stability; Discontinuous solutions

☆ This work is supported by the project "Adaptive error analysis for non-stationary hyperbolic systems in reactive and multi-phase flow", contract # DFG WA 633/10-3.

* Corresponding author. Tel.: +49-391-6712877; fax: +49-391-6718073.
E-mail addresses: matthias.kunik@mathematik.uni-magdeburg.de (M. Kunik), shamsul.qamar@mathematik.uni-magdeburg.de (S. Qamar), gerald.warnecke@mathematik.uni-magdeburg.de (G. Warnecke).

0021-9991/$ - see front matter
doi:10.1016/j.jcp.2003.07.019

1. Introduction

In modeling flow at speeds where relativistic effects become important, space and time are intrinsically coupled and the Euler equations of gas dynamics become more complicated. However, it is still possible to write the relativistic Euler equations as a first-order hyperbolic system that can be advanced forward in time in some fixed reference frame. We call the reference frame a laboratory frame since this is typically the frame from which we are observing. Relativistic gas dynamics plays an important role in areas of astrophysics, high energy particle beams, high energy nuclear collisions, and free-electron laser technology.

There are two approaches to solve the Euler equations numerically. One is based on the Euler equations, for example Godunov-type schemes and central schemes. While the other approach is based on the transport equations, for example kinetic schemes. In the kinetic schemes the moments of the Maxwellian phase density are used in order to derive the constitutive relations. Using the conservation laws these constitutive relations lead to the Euler equations. This distinction in the solution approaches was first made by Harten et al. [19]. No matter how a numerical scheme for the Euler equations is derived we expect it to have certain properties apart from being consistent with the equations. Due to the presence of discontinuities and weak solutions *convergence* is very difficult to prove. Some convergence results are available for scalar hyperbolic equations and for special 2×2 systems, however, no such result exist for the Euler equations. Other properties are needed to ascertain good quality of the numerical solution: the numerical scheme should be robust in handling discontinuities, and it should show no grid dependencies in multi-dimensions. In addition, it should retain properties specific to the Euler equations: conservation of mass, momentum, and energy, positivity of density and pressure, and entropy inequalities. We will show in this study that kinetic schemes preserve all these properties.

Kinetic approaches in order to solve the non-relativistic Euler equations of gas dynamics were successfully applied to several initial and boundary value problems, see for example [7–10,32,35–37]. Some interesting links between the Euler system and the so-called kinetic BGK-model, which was introduced by Bhatnagar et al. [1], are discussed in the textbooks by Cercignani [3], Cercignani et al. [4] as well as by Godlewski and Raviart [15].

Kunik et al. have used the kinetic schemes in order to solve the relativisic Euler equations, see [24,25]. These kinetic schemes are discrete in time but continuous in space. Also, these schemes are unconditionally stable as they do not require any CFL condition. We have also used first and second-order BGK-type kinetic flux vector splitting (KFVS) schemes in order to solve the one- and two-dimensional ultra-relativistic Euler equations, see [26]. Further, we have applied the basic idea of these works to the evolution of temperature and heat flux in a Bose gas of phonons, see [27].

A characteristic feature of kinetic theory is that its models are statistical and the particle systems are described by distribution functions $f = f(t, \mathbf{x}, \mathbf{q})$, which represent the density of particles and momenta with given space–time position $(t, \mathbf{x}) \in \mathbb{R} \times \mathbb{R}^3$ and momentum $\mathbf{q} \in \mathbb{R}^3$. A distribution function contains a wealth of information, and macroscopical quantities are easily calculated from this function. These macroscopic quantities do not depend on the momentum $\mathbf{q}$ but only on the space–time point $(t, \mathbf{x})$. In kinetic theory the time evolution of the system is determined by the interactions between the particles which depend on the physical situation. For instance, the driving mechanism for the time evolution of a neutral gas is the collision between particles, the relativistic Boltzmann equation. For a plasma the interaction is through the electric charges, the Vlasov–Maxwell system, and in the stellar and cosmological cases the interaction is gravitational, the Einstein–Vlasov system. Of course, combinations of interaction processes are also considered but in many situations one of them is strongly dominating and the weaker processes are neglected.

A few years after Einstein's famous paper "Zur Elektrodynamik bewegter Körper", Jüttner [21] extended the kinetic theory of gases which was developed by D. Bernoulli, Clausius, Maxwell and Boltzmann, to the domain of relativity. He succeeded in deriving the relativistic generalization of the Maxwellian equilibrium phase density. Later on this phase density and the whole relativistic kinetic theory was

structured in a well organized Lorentz-invariant form, see [5,6,20], and the textbook of deGroot et al. [17]. Jüttner [22] also established the relativistic form of equilibrium phase densities and the corresponding equations of state for the systems of bosons and fermions. In the textbook of Weinberg [34] one can find a short introduction to special relativity and relativistic hydrodynamics with further literature also for the imperfect fluid (gas), see for example the papers of Eckart [12–14]. A good introduction about the recent methods applied to relativistic gas dynamics can be found in the review article of Martí and Müller [23]. It is noted that, except the *kinetic beam scheme* of Yang et al. [38], all other methods developed for the relativistic Euler equations are based on macroscopic continuum description.

In this paper we extend our first-order kinetic scheme (continuous in space) to second order for the one-dimensional ultra-relativistic Euler equations, see [24]. Deshpande [8] has used a similar approach in order to get second-order accuracy of the kinetic scheme for the non-relativistic Euler equations. Similar to the non-relativistic case [8], a fascinating aspect of the present work is the use of antidiffusive Chapmann–Enskog theory in the development of the second-order accurate kinetic scheme. Normally the Chapmann–Enskog theory is associated with the Navier–Stokes equations. We show that to cancel the large amount of viscosity in the first-order kinetic scheme, antidiffusive terms are required, and these can be introduced through the Chapmann–Enskog-type relativistic phase density. We also extend the kinetic scheme to account for the boundary conditions. The application of the boundary conditions are different from other finite-difference methods. The boundary conditions are at the level of the velocity distribution function, which is natural in the kinetic scheme. This second-order kinetic scheme is applied to several one-dimensional problems, and the results demonstrate the capability of the method for giving 'wiggle-free' accurate solutions.

Now we give a short overview of this article:

In Section 2 we will present the basic definitions of the relativistic kinetic theory, namely the macroscopic quantities considered in thermodynamics which are obtained from a kinetic phase density. Moreover the relativistic Maxwellian in the ultra-relativistic case is introduced, see [24].

In Section 3 we calculate the macroscopic moments of the relativistic Maxwellian in order to formulate the ultra-relativistic Euler equations as conservation laws for the particle number, momentum, and energy. The Euler equations are written in differential form as well as in a weak integral form. An entropy inequality is given in weak integral form with an entropy function which satisfies the Gibbs equation.

In Section 4 we first formulate the first-order kinetic scheme in order to solve the three-dimensional ultra-relativistic Euler equations, see [24]. The conservation laws and the entropy inequality for the scheme were proved in [24]. Here we also prove the positivity and L^1-stability of the kinetic scheme. In contrast to the classical three-dimensional Euler equations for a non-relativistic gas we will show that the threefold momentum integrals for the particle-density four-vector and for the energy–momentum tensor reduce simply to surface integrals where the integration is performed with respect to the unit sphere. A similar idea was used by [11,27] in order to solve the hyperbolic moment systems for a phonon Bose-gas, resulting from the Boltzmann–Peierls equation and maximum entropy principle.

In Section 5 we are looking at the special case of spatially one-dimensional solutions which are nevertheless solutions to the three-dimensional ultra-relativistic Euler equations. In this case the surface integrals of the three-dimensional kinetic scheme reduce again to single integrals which range from -1 to $+1$. They indicate the finite domain of dependence on the preceding initial data, which is covered by the backward light-cones, see [24]. This property does not hold for classical kinetic schemes. We explain the numerical implementation of the scheme. We also explain how to extend the scheme to initial and boundary value problems. In order to calculate the free-flight phase density we use an interpolation polynomial for which total variation diminishing (TVD) property was proved by Deshpande [8] in the non-relativistic case. The proof of the TVD property in the relativistic case is exactly the same with minor modifications, therefore we omit the proof in this paper.

In Section 6 we extend the one-dimensional first-order kinetic scheme to second order by using the approach of Deshpande [8]. We use two approaches in order to get second-order accuracy in time. Both

approaches lead to the same results. To get second-order accuracy we use second order in space interpolation polynomial for the calculation of the free-flight phase density. This interpolation polynomial also satisfies the TVD property, see [8].

In Section 7 we report computations for numerical test cases. We compare the kinetic scheme results with that of Godunov [16] and central schemes of Nessayahu and Tadmor [28]. The CFL condition for central and upwind schemes in the ultra-relativistic case is very simple which is $\Delta t = \Delta x/2$. This CFL condition comes out automatically due to the structure of light cones, since every signal speed is bounded by the velocity of light. We also check the experimental order of convergence (EOC) and numerical L^1-error for the first and second-order kinetic schemes by using smooth initial data.

2. The relativistic kinetic theory

In this section we describe a relativistic gas consisting of many microscopic structureless particles in terms of the relativistic kinetic phase density. From this fundamental phase density we calculate tensorial moments which give the local macroscopic physical quantities of the gas such as the particle density, the velocity, the pressure, the temperature and so on.

In order to formulate the theory in a Lorentz-invariant form, we make use of the notations for the tensor calculus used in the textbook of Weinberg [34], with only slight modifications:

(A) *The space–time coordinates* are x^μ, $\mu = 0, 1, 2, 3$, with $x^0 := ct$ for the time, x^1, x^2, x^3 for the position.

(B) *The metric-tensor* is

$$g_{\mu\nu} = g^{\mu\nu} = \begin{cases} +1, & \mu = \nu = 0, \\ -1, & \mu = \nu = 1, 2, 3, \\ 0, & \mu \neq \nu. \end{cases} \tag{2.1}$$

(C) *The proper Lorentz-transformations* are linear transformations Λ^α_β from one system of space–time with coordinates x^α to another system x'^α. They must satisfy

$$x'^\alpha = \Lambda^\alpha_\beta x^\beta, \quad g_{\mu\nu} = \Lambda^\alpha_\mu \Lambda^\beta_\nu g_{\alpha\beta}, \quad \Lambda^0_0 \geqslant 1, \quad \det \Lambda = +1. \tag{2.2}$$

The conditions $\Lambda^0_0 \geqslant 1$ and $\det \Lambda = +1$ are necessary in order to exclude inversion in time and space. Then the following quantity forms a tensor with respect to proper Lorentz-transformations, the so-called Levi-Civita tensor:

$$\epsilon_{\alpha\beta\gamma\delta} = \begin{cases} +1, & \alpha\beta\gamma\delta \text{ even permutation of } 0123, \\ -1, & \alpha\beta\gamma\delta \text{ odd permutation of } 0123, \\ 0, & \text{otherwise.} \end{cases}$$

Note that in the textbook of Weinberg [34] this tensor as well as the metric tensor both take the sign opposite to the notation used here.

(D) *Einstein's summation convention*. Any Greek index like α, β that appears twice, once as a subscript and once as a superscript, is understood to be summed over $0, 1, 2, 3$ if not noted otherwise. For spatial indices, which are denoted by Latin indices like i, j, k, we will not apply this summation convention.

Now we take a microscopic look at the gas and start with the kinematics of a representative gas atom with particle trajectory $\mathbf{x} = \mathbf{x}(t)$, where the time coordinate t and the space coordinate $\mathbf{x}$ are related to an arbitrary Lorentz-frame. The invariant mass of all structureless particles is assumed to be the same and is denoted by m_0. The microscopic velocity of the gas atom is $\mathrm{d}\mathbf{x}(t)/\mathrm{d}t$, and its microscopic velocity four-vector is given by cq^μ, where the *dimensionless microscopic velocity four-vector* q^μ is defined by

$$(q^0, \mathbf{q})^{\mathrm{T}}, \quad q^0 = q_0 = \sqrt{1+\mathbf{q}^2}, \quad \mathbf{q} = \frac{\frac{1}{c}\frac{\mathrm{d}\mathbf{x}}{\mathrm{d}t}}{\sqrt{1-\left(\frac{1}{c}\frac{\mathrm{d}\mathbf{x}}{\mathrm{d}t}\right)^2}}. \tag{2.3}$$

Note that in the ultra relativistic case $q^0 = |\mathbf{q}|$, see [24,25] for further details.

The *relativistic phase density* $f(t, \mathbf{x}, \mathbf{q}) \geqslant 0$ is the basic quantity of the kinetic theory. This function may be interpreted as giving the average number of particles with certain momentum at each time–space point. In the following we make use of the fact that the so-called *volume element* d^3q/q_0 is invariant with respect to Lorentz-transformations.

Now we give the following definitions for the macroscopic moments and entropy four-vector and the definition of the macroscopic basic fields which we need for the formulation of the ultra-relativistic Euler equations, for more details see [24,25].

(i) *Particle-density four-vector*:

$$N^\mu = N^\mu(t, \mathbf{x}) = \int_{\mathbb{R}^3} q^\mu f(t, \mathbf{x}, \mathbf{q}) \frac{\mathrm{d}^3 q}{q^0}. \tag{2.4}$$

(ii) *Energy–momentum tensor*:

$$T^{\mu\nu} = T^{\mu\nu}(t, \mathbf{x}) = m_0 c^2 \int_{\mathbb{R}^3} q^\mu q^\nu f(t, \mathbf{x}, \mathbf{q}) \frac{\mathrm{d}^3 q}{q^0} \tag{2.5}$$

with $\mu, \nu = 0, 1, 2, 3$, i.e. these are total 16 quanties.

(iii) *Entropy four-vector*:

$$S^\mu = S^\mu(t, \mathbf{x}) = -k_{\mathrm{B}} \int_{\mathbb{R}^3} q^\mu f(t, \mathbf{x}, \mathbf{q}) \ln\left(\frac{f(t, \mathbf{x}, \mathbf{q})}{\chi}\right) \frac{\mathrm{d}^3 q}{q^0}. \tag{2.6}$$

Here $k_{\mathrm{B}} = 1.38062 \times 10^{-23}$ J/K is Boltzmann's constant and $\chi = (\frac{m_0 c}{\hbar})^3$ with Planck's constant $\hbar = 1.05459 \times 10^{-34}$ J s. Note that χ has the same dimension as f, namely 1/volume.

Tensor algebraic combinations of these moments:

(i) *The particle density*

$$n = \sqrt{N^\mu N_\mu}, \tag{2.7}$$

(ii) *the dimensionless velocity four-vector*

$$u^\mu = \frac{1}{n} N^\mu, \tag{2.8}$$

(iii) *the pressure and temperature*

$$p = \frac{1}{3}(u_\mu u_\nu - g_{\mu\nu}) T^{\mu\nu} = k_{\mathrm{B}} n T. \tag{2.9}$$

Remark. The *macroscopic velocity* $\mathbf{v}$ of the gas can be obtained easily from the spatial part $\mathbf{u} = (u^1, u^2, u^3)^{\mathrm{T}}$ of the dimensionless velocity four-vector by

$$\mathbf{v} = c \frac{\mathbf{u}}{\sqrt{1+\mathbf{u}^2}}. \tag{2.10}$$

From this formula we can immediately read off that $|\mathbf{v}| < c$, i.e. the absolute value of the velocity is bounded by the speed of light. Note also that $u^0 = \sqrt{1+\mathbf{u}^2}$ is the Lorentz factor $1/\sqrt{1-\mathbf{v}^2/c^2}$. These definitions are valid for any relativistic phase-density $f = f(t, \mathbf{x}, \mathbf{q})$.

The most interesting aspect of the kinetic schemes is that instead of dealing with a system of nonlinear hyperbolic partial differential equations (for example relativistic Euler equations), we consider the collisionless transport equation of the kinetic theory of gases for developing upwind schemes. This relativistic linear transport equation without collision term

$$\frac{1}{c}\frac{\partial f}{\partial t} + \sum_{k=1}^{3} \frac{q^k}{q^0}\frac{\partial f}{\partial x^k} = 0 \tag{2.11}$$

is a linear transport equation for the scalar f. This equation gives the following conservation laws for the particle number, momentum and energy in differential form

$$\frac{\partial N^\mu}{\partial x^\mu} = 0, \quad \frac{\partial T^{\mu\nu}}{\partial x^\mu} = 0, \qquad \mu, \nu = 0, 1, 2, 3. \tag{2.12}$$

Jüttner extended the classical velocity distribution of Maxwell for a gas in equilibrium to the relativistic case. The resulting *Jüttner distribution* $f_{\mathrm{J}}(n, T, \mathbf{u}, \mathbf{q})$ depends on five constant parameters, which describe the state of the gas in equilibrium, namely the particle density n, the absolute temperature T and the spatial part $\mathbf{u} \in \mathbb{R}^3$ of the dimensionless four-velocity, see [24,25]. The Jüttner phase density in the ultra-relativistic limit [24] is given by

$$f_{\mathrm{J}}^*(n, T, \mathbf{u}, \mathbf{q}) = \frac{n}{8\pi T^3}\exp\left(-\frac{u_\mu q^\mu}{T}\right) = \frac{n}{8\pi T^3}\exp\left(-\frac{|\mathbf{q}|}{T}\left(\sqrt{1+\mathbf{u}^2} - \mathbf{u}\cdot\frac{\mathbf{q}}{|\mathbf{q}|}\right)\right), \tag{2.13}$$

where in the ultra-relativistic limit

$$q^0 = q_0 = |\mathbf{q}|. \tag{2.14}$$

From the generally valid formula (2.9) for the pressure, we have

$$p = \frac{1}{3}u_\mu u_\nu T^{\mu\nu} - \frac{1}{3}g_{\mu\nu}T^{\mu\nu} = \frac{1}{3}u_\mu u_\nu T^{\mu\nu} - \int_{\mathbb{R}^3} g_{\mu\nu}q^\mu q^\nu f\frac{\mathrm{d}^3 q}{q^0}. \tag{2.15}$$

Since $g_{\mu\nu}q^\mu q^\nu = q_\nu q^\nu = 0$ holds due to (2.14), we immediately conclude that

$$p = \frac{e}{3} = \frac{1}{3}T^{\mu\nu}u_\mu u_\nu = nT, \tag{2.16}$$

in the ultra-relativistic case.

Further, when the basic unknown f in (2.11), the distribution function, is replaced by the relativistic Jüttner distribution function, see [24,25], then the collisionless transport equation (2.11) is in general no longer valid, whereas the conservation laws (2.12) are still satisfied and will reduce to the relativistic Euler equations. Apart from this if we take into account shock discontinuity then we need the weak form of conservation laws and entropy inequality as given below:

$$\oint_{\partial\Omega} N^\nu(t, \mathbf{x})\,\mathrm{d}o_\nu = 0, \quad \oint_{\partial\Omega} T^{\mu\nu}(t, \mathbf{x})\,\mathrm{d}o_\nu = 0, \quad \oint_{\partial\Omega} S^\nu(t, \mathbf{x})\,\mathrm{d}o_\nu \geqslant 0. \tag{2.17}$$

Here the covariant vector $\mathrm{d}o_\nu$ is a positively oriented surface element on the boundary $\partial\Omega$. It can be written in covariant form as

$$\mathrm{d}o_\kappa = \varepsilon_{\kappa\lambda\mu\nu} \sum_{i,j,m=1}^{3} \frac{\partial x^\lambda}{\partial u^i} \frac{\partial x^\mu}{\partial u^j} \frac{\partial x^\nu}{\partial u^m} \mathrm{d}u^i \mathrm{d}u^j \mathrm{d}u^m,$$

where $x^\alpha = x^\alpha(u^1, u^2, u^3)$ is a positively oriented parameterization of the boundary $\partial\Omega$.

In the following we will only consider dimensionless physical quantities corresponding to $k_\mathrm{B} = 1$, $\hbar = 1$ and $c = 1$. Also we will use $|\mathbf{q}|$ in place of $q^0 = q_0$.

3. The ultra-relativistic Euler equations

Using the ultra-relativistic Jüttner distribution (2.13) we obtain from the dimensionless form of the moments (2.4)–(2.6)

$$N^\mu = nu^\mu, \quad T^{\mu\nu} = -pg^{\mu\nu} + 4pu^\mu u^\nu, \tag{3.1}$$

$$S^\mu = -N^\mu \ln\frac{n^4}{p^3} + \gamma N^\mu, \quad \sigma = -n\ln\frac{n^4}{p^3} + \gamma n, \tag{3.2}$$

where γ may be any real dimensionless constant. Note that due to the mass conservation (2.12) the divergence of S^μ, which will give rise to the H-theorem formulated later, will not change when we add some multiple of N^μ to S^μ. Moreover σ obeys the Gibbs equation

$$T\,\mathrm{d}\left(\frac{\sigma}{n}\right) = p\,\mathrm{d}\left(\frac{1}{n}\right) + \mathrm{d}\left(\frac{e}{n}\right). \tag{3.3}$$

These formulas can be easily checked for a special Lorentz frame where $u^0 = 1$, $u^1 = u^2 = u^3 = 0$, i.e. where the gas is locally at rest. Since the ultra-relativistic moments (3.1) are valid in a special Lorentz frame and since these equations are written in tensor invariant form, they are generally valid in every Lorentz frame. Using the moments (3.1) and the conservation laws (2.12), we get at regular points the three-dimensional Euler equation in differential form

$$\frac{\partial}{\partial t}(n\sqrt{1+\mathbf{u}^2}) + \nabla\cdot(n\mathbf{u}) = 0, \tag{3.4}$$

$$\frac{\partial}{\partial t}(4pu^i\sqrt{1+\mathbf{u}^2}) + \sum_{k=1}^{3}\frac{\partial}{\partial x^k}(p\delta^{ik} + 4pu^iu^k) = 0, \tag{3.5}$$

$$\frac{\partial}{\partial t}(3p + 4p\mathbf{u}^2) + \sum_{k=1}^{3}\frac{\partial}{\partial x^k}(4pu^k\sqrt{1+\mathbf{u}^2}) = 0. \tag{3.6}$$

At regular points the function is continuously differentiable with respect to time and space. Note that Eqs. (3.5) and (3.6) are a closed 4 by 4 system for p and $\mathbf{u}$. The relativistic continuity equation (3.4) decouples from the system. For given $\mathbf{u}$ it is a scalar equation for n.

In order to get the primitive variables we solve the equations

$$\begin{aligned} N^0(t,\mathbf{x}) &= n(t,\mathbf{x})\sqrt{1+\mathbf{u}^2(t,\mathbf{x})},\\ T^{0k}(t,\mathbf{x}) &= 4p(t,\mathbf{x})u^k(t,\mathbf{x})\sqrt{1+\mathbf{u}^2(t,\mathbf{x})},\\ T^{00}(t,\mathbf{x}) &= p(t,\mathbf{x})[3+4\mathbf{u}^2(t,\mathbf{x})], \end{aligned} \tag{3.7}$$

for $p = nT$, $\mathbf{u}$, and n. This gives

$$\begin{aligned} p(t,\mathbf{x}) &= \frac{1}{3}\left[-T^{00} + \sqrt{4(T^{00})^2 - 3\sum_{k=1}^{3}(T^{0k})^2}\right], \\ u^k(t,\mathbf{x}) &= \frac{T^{0k}}{\sqrt{4p(t,\mathbf{x})[p(t,\mathbf{x}) + T^{00}]}}, \quad n(t,\mathbf{x}) = \frac{N^0}{\sqrt{1+\sum_{k=1}^{3}[u^k(t,\mathbf{x})]^2}}. \end{aligned} \tag{3.8}$$

Now we are looking for special solutions of the three-dimensional ultra-relativistic Euler equations, which will not depend on x^2, x^3 but only on $x = x^1$. Moreover we restrict to a one-dimensional flow field $\mathbf{u} = (u(t,x),0,0)^{\mathrm{T}}$,

$$\begin{aligned} &(n\sqrt{1+u^2})_t + (nu)_x = 0, \\ &(4pu\sqrt{1+u^2})_t + (p(1+4u^2))_x = 0, \\ &(p(3+4u^2))_t + (4pu\sqrt{1+u^2})_x = 0. \end{aligned} \tag{3.9}$$

In a one-dimensional case we know from the constitutive relations (3.1) that

$$\begin{pmatrix} N^0 \\ T^{01} \\ T^{00} \end{pmatrix} = \begin{pmatrix} n\sqrt{1+u^2} \\ 4pu\sqrt{1+u^2} \\ p(3+4u^2) \end{pmatrix}, \quad \begin{pmatrix} N^1 \\ T^{11} \\ T^{01} \end{pmatrix} = \begin{pmatrix} nu \\ p(1+4u^2) \\ 4pu\sqrt{1+u^2} \end{pmatrix}. \tag{3.10}$$

The differential equations (3.9) constitute a strictly hyperbolic system with the characteristic velocities

$$\lambda_1 = \frac{2u\sqrt{1+u^2} - \sqrt{3}}{3+2u^2}, \quad \lambda_2 = \frac{u}{\sqrt{1+u^2}}, \quad \lambda_3 = \frac{2u\sqrt{1+u^2} + \sqrt{3}}{3+2u^2}. \tag{3.11}$$

These eigenvalues may first be obtained in the Lorentz rest frame where $u = 0$. Then using the relativistic additivity law for the velocities, we can easily obtain (3.11) in the general Lorentz frame. In the Lorentz rest frame we obtain the positive speed of sound $\lambda = \frac{1}{\sqrt{3}}$, which is independent of the spatial direction.

The differential equations (3.9) are not sufficient if we take shock discontinuities into account. Therefore we choose a weak integral formulation which is given due to Oleinik [30] by curve integrals in time and space, namely

$$\begin{aligned} &\oint_{\partial\Omega} n\sqrt{1+u^2}\,\mathrm{d}x - nu\,\mathrm{d}t = 0, \\ &\oint_{\partial\Omega} 4pu\sqrt{1+u^2}\,\mathrm{d}x - p(1+4u^2)\,\mathrm{d}t = 0, \\ &\oint_{\partial\Omega} p(3+4u^2)\,\mathrm{d}x - 4pu\sqrt{1+u^2}\,\mathrm{d}t = 0. \end{aligned} \tag{3.12}$$

Here $\Omega \subset \mathbb{R}_0^+ \times \mathbb{R}$ is a normal region in space–time and with a piecewise smooth, positively oriented boundary. Note that this weak formulation takes discontinuities into account, since there are no derivatives of the fields involved. The use of Oleinik's formulation enables a direct proof of conservation laws and entropy inequality, see [24]. If we apply the Gaussian divergence theorem to the weak formulation (3.12) in time–space regions where the solution is regular we come back to the differential equation form of the Euler equations (3.9).

Furthermore we require that the weak solution (3.12) must also satisfy the *entropy-inequality*

$$\oint_{\partial\Omega} S^0\,\mathrm{d}x - S^1\,\mathrm{d}t \geqslant 0, \tag{3.13}$$

where

$$S^0 = -n\sqrt{1+u^2}\ln\frac{n^4}{p^3}, \quad S^1 = -nu\ln\frac{n^4}{p^3}. \tag{3.14}$$

4. Three-dimensional first-order kinetic scheme

We first formulate the scheme for the three-dimensional Euler equations. After that we solve the one-dimensional Euler equations, using a special integration technique. Recalling the ultra-relativistic Jüttner phase density (2.13), we start with the given initial data $n_{\mathrm{I}}(\mathbf{x}) = n(0,\mathbf{x})$, $T_{\mathrm{I}}(\mathbf{x}) = T(0,\mathbf{x})$, $u_{\mathrm{I}}(\mathbf{x}) = u(0,\mathbf{x})$. We prescribe a time step $\tau_M > 0$ and let $t_n = n\tau_M$ for $n = 0,1,2,3,\ldots$ be the maximization times. Then the kinetic scheme in three-space dimensions is given by

$$\begin{aligned}
N^{\mu}(t_n+\tau_M,\mathbf{x}) &= \int_{\mathbb{R}^3} q^{\mu} f_n\left(\mathbf{x}-\tau_M\frac{\mathbf{q}}{|\mathbf{q}|},\mathbf{q}\right)\frac{\mathrm{d}^3q}{|\mathbf{q}|},\\
T^{\mu\nu}(t_n+\tau_M,\mathbf{x}) &= \int_{\mathbb{R}^3} q^{\mu}q^{\nu} f_n\left(\mathbf{x}-\tau_M\frac{\mathbf{q}}{|\mathbf{q}|},\mathbf{q}\right)\frac{\mathrm{d}^3q}{|\mathbf{q}|},\\
S^{\mu}(t_n+\tau_M,\mathbf{x}) &= -\int_{\mathbb{R}^3} q^{\mu}(f_n\ln f_n)\left(\mathbf{x}-\tau_M\frac{\mathbf{q}}{|\mathbf{q}|},\mathbf{q}\right)\frac{\mathrm{d}^3q}{|\mathbf{q}|},
\end{aligned} \tag{4.1}$$

with the ultra-relativistic initial phase density at the maximization time t_n given as

$$f_n(\mathbf{y},\mathbf{q}) = f_{\mathrm{J}}^*(n(t_n,\mathbf{y}),T(t_n,\mathbf{y}),\mathbf{u}(t_n,\mathbf{y}),\mathbf{q}). \tag{4.2}$$

Moreover n, T, u^{μ} are calculated from N^{μ} and $T^{\mu\nu}$ for the next time step by using the relations (3.8).

Further, we can apply an important simplification of the volume integrals $(4.1)_{1,2}$ for the free-flight moments, see [24]. We can see in (4.2) that the fields $n(t,\mathbf{y})$, $T(t,\mathbf{y})$ and $\mathbf{u}(t,\mathbf{y})$ are not depending on $|\mathbf{q}|$ but only on the unit vector $\mathbf{w} = (w^1,w^2,w^3)^{\mathrm{T}} = \mathbf{q}/|\mathbf{q}|$. This fact enables us to reduce the three-fold volume integrals to the twofold surface integrals by applying polar coordinates. Using the abbreviations

$$\begin{aligned}
\Phi(\mathbf{y},\mathbf{w}) &= \frac{1}{4\pi}\frac{n(\mathbf{y})}{\left(\sqrt{1+\mathbf{u}^2(\mathbf{y})}-\mathbf{w}\cdot\mathbf{u}(\mathbf{y})\right)^3},\\
\Psi(\mathbf{y},\mathbf{w}) &= \frac{3}{4\pi}\frac{(nT)(\mathbf{y})}{\left(\sqrt{1+\mathbf{u}^2(\mathbf{y})}-\mathbf{w}\cdot\mathbf{u}(\mathbf{y})\right)^4},
\end{aligned} \tag{4.3}$$

we can now carry out the integration with respect to $|\mathbf{q}|$ explicitly and obtain the following reduced surface integrals for the moments:

$$\begin{aligned}
N^{\mu}(t_n+\tau_M,\mathbf{x}) &= \oint_{\partial B(1,0)} w^{\mu}\Phi(\mathbf{x}-\tau_M\mathbf{w},\mathbf{w})\,\mathrm{d}S(\mathbf{w}),\\
T^{\mu\nu}(t_n+\tau_M,\mathbf{x}) &= \oint_{\partial B(1,0)} w^{\mu}w^{\nu}\Psi(\mathbf{x}-\tau_M\mathbf{w},\mathbf{w})\,\mathrm{d}S(\mathbf{w}),
\end{aligned} \tag{4.4}$$

where $w^0 = 1$ and $\mathbf{w} = \mathbf{q}/|\mathbf{q}|$ is the unit vector in direction of $\mathbf{q}$ and $B(r, \mathbf{x}_0)$ is the ball with radius r and center $\mathbf{x}_0$. Its boundary is the sphere $\partial B(r, \mathbf{x}_0)$. These surface integrals reflect the fact that in the ultra-relativistic case the particles are moving on the surface of the light cone.

Proposition 4.1. *Let $0 < \tau < \tau_M$ and $n = 0, 1, 2, \ldots$ We consider the moments in the free-flight between the two maximization times t_n and t_{n+1}. Within this free-flight zone the moments $N^\mu(t_n + \tau, \mathbf{x})$, $T^{\mu\nu}(t_n + \tau, \mathbf{x})$ and the entropy four-vector $S^\mu(t_n + \tau, \mathbf{x})$ satisfy the following conservation laws in weak integral form*:

$$\oint_{\partial\Omega} N^\nu(t_n + \tau, \mathbf{x})\, \mathrm{d}o_\nu = 0, \quad \oint_{\partial\Omega} T^{\mu\nu}(t_n + \tau, \mathbf{x})\, \mathrm{d}o_\nu = 0, \quad \oint_{\partial\Omega} S^\nu(t_n + \tau, \mathbf{x})\, \mathrm{d}o_\nu = 0.$$

Here the covariant vector $\mathrm{d}o_\nu$ is a positively oriented surface element to the boundary $\partial\Omega$. It can be written in covariant form as

$$\mathrm{d}o_\kappa = \varepsilon_{\kappa\lambda\mu\nu} \sum_{i,j,m=1}^{3} \frac{\partial x^\lambda}{\partial u^i} \frac{\partial x^\mu}{\partial u^j} \frac{\partial x^\nu}{\partial u^m}\, \mathrm{d}u^i\, \mathrm{d}u^j\, \mathrm{d}u^m,$$

where $x^\alpha = x^\alpha(u^1, u^2, u^3)$ is a positively oriented parameterization of the boundary $\partial\Omega$.

Remark. Note that these weak formulations correspond to the differential equations

$$\frac{\partial N^\nu}{\partial x^\nu}(t_n + \tau, \mathbf{x}) = 0, \quad \frac{\partial T^{\mu\nu}}{\partial x^\nu}(t_n + \tau, \mathbf{x}) = 0, \quad \frac{\partial S^\nu}{\partial x^\nu}(t_n + \tau, \mathbf{x}) = 0. \tag{4.5}$$

Proof. To see the proof, the reader is referred to our article [24]. □

Proposition 4.2. *Let $\Omega \subset \mathbb{R}_0^+ \times \mathbb{R}^3$ be any bounded convex region in time and space. By $\mathrm{d}o_\nu$ we denote the positively oriented surface element of $\partial\Omega$. Let $\tau_M > 0$ be a fixed time step. The moment representations* (4.1) *calculated by the iterated scheme defined above have the following properties*:

(i) *The conservation laws for the particle number, the momentum and energy hold, i.e.*

$$\oint_{\partial\Omega} N^\nu\, \mathrm{d}o_\nu = 0, \quad \oint_{\partial\Omega} T^{\mu\nu}\, \mathrm{d}o_\nu = 0. \tag{4.6}$$

(ii) *The following entropy inequality is satisfied*

$$\oint_{\partial\Omega} S^\nu\, \mathrm{d}o_\nu \geqslant 0. \tag{4.7}$$

Proof. For the proof see our article [24]. □

4.1. Positivity and L^1-stability of the kinetic scheme

Here we show that our kinetic scheme preserves positivity of the density and pressure.

Theorem 4.1. *Assume that the initial distribution function satisfies $f_n(\mathbf{y}, \mathbf{q}) \geqslant 0$, additionally $f_n(\mathbf{y}, \mathbf{q})$ does not vanish almost everywhere for all microscopic velocities $\mathbf{q}$, macroscopic velocities $\mathbf{u}$, positive densities n and pressures p. Then the numerical solution obtained by the resulting kinetic scheme has the following property*: *Its density, pressure and total energy remain positive for all times*:

$$n(t_n+\tau,\mathbf{x})>0,\quad p(t_n+\tau,\mathbf{x})=\frac{1}{3}e(t_n+\tau,\mathbf{x})>0,\quad E(t_n+\tau,\mathbf{x})>0. \tag{4.8}$$

This also means that the numerical scheme defined by (4.1) *is stable in* L^1.

Proof. Since the particle density is defined as $n=\sqrt{N^\mu N_\mu}$, we have to prove that

$$N^\mu N_\mu(t_n+\tau,\mathbf{x})=((N^0)^2-(N^1)^2-(N^2)^2-(N^3)^2)(t_n+\tau,\mathbf{x})>0. \tag{4.9}$$

According to the Cauchy–Schwarz inequality, if we have two functions f and g then

$$\left(\int_a^b f\cdot g\,\mathrm{d}x\right)^2\leqslant\left(\int_a^b f^2\,\mathrm{d}x\right)\cdot\left(\int_a^b g^2\,\mathrm{d}x\right), \tag{4.10}$$

where equality holds iff the functions f and g are linearly dependent.

From the moments $(4.1)_1$, we have

$$N^0(t_n+\tau,\mathbf{x})=\int_{\mathbb{R}^3} f_n\left(\mathbf{x}-\tau\frac{\mathbf{q}}{|\mathbf{q}|},\mathbf{q}\right)\mathrm{d}^3q>0. \tag{4.11}$$

Using again the free-flight moments $(4.1)_1$ and the Cauchy–Schwarz inequality, we get

$$\begin{aligned}(N^1)^2(t_n+\tau,\mathbf{x})&=\left(\int_{\mathbb{R}^3} q^1 f_n\left(\mathbf{x}-\tau\frac{\mathbf{q}}{|\mathbf{q}|},\mathbf{q}\right)\frac{\mathrm{d}^3q}{|\mathbf{q}|}\right)^2\\&=\left(\int_{\mathbb{R}^3}\left(\left(\frac{q^1}{|\mathbf{q}|}\sqrt{f_n}\right)\cdot\left(\sqrt{f_n}\right)\right)\left(\mathbf{x}-\tau\frac{\mathbf{q}}{|\mathbf{q}|},\mathbf{q}\right)\mathrm{d}^3q\right)^2\\&<\left(\int_{\mathbb{R}^3}\left(\frac{q^1}{|\mathbf{q}|}\sqrt{f_n}\right)^2\left(\mathbf{x}-\tau\frac{\mathbf{q}}{|\mathbf{q}|},\mathbf{q}\right)\mathrm{d}^3q\right)\cdot\left(\int_{\mathbb{R}^3}\left(\sqrt{f_n}\right)^2\left(\mathbf{x}-\tau\frac{\mathbf{q}}{|\mathbf{q}|},\mathbf{q}\right)\mathrm{d}^3q\right)\\&=N^0(t_n+\tau,\mathbf{x})\left(\int_{\mathbb{R}^3}\left(\frac{q^1}{|\mathbf{q}|}\right)^2 f_n\left(\mathbf{x}-\tau\frac{\mathbf{q}}{|\mathbf{q}|},\mathbf{q}\right)\mathrm{d}^3q\right).\end{aligned} \tag{4.12}$$

In Cauchy–Schwarz inequality we have not taken the equality sign, because the functions $\frac{q^1}{|\mathbf{q}|}\sqrt{f_n(\mathbf{y},\mathbf{q})}$ and $\sqrt{f_n(\mathbf{y},\mathbf{q})}$ are linearly independent. Similarly

$$\begin{aligned}(N^2)^2(t_n+\tau,\mathbf{x})&<N^0(t_n+\tau,\mathbf{x})\left(\int_{\mathbb{R}^3}\left(\frac{q^2}{|\mathbf{q}|}\right)^2 f_n\left(\mathbf{x}-\tau\frac{\mathbf{q}}{|\mathbf{q}|},\mathbf{q}\right)\mathrm{d}^3q\right),\\(N^3)^2(t_n+\tau,\mathbf{x})&<N^0(t_n+\tau,\mathbf{x})\left(\int_{\mathbb{R}^3}\left(\frac{q^3}{|\mathbf{q}|}\right)^2 f_n\left(\mathbf{x}-\tau\frac{\mathbf{q}}{|\mathbf{q}|},\mathbf{q}\right)\mathrm{d}^3q\right).\end{aligned} \tag{4.13}$$

Now we use (4.12) and (4.13) in (4.9). Also in the ultra-relativistic case

$$|\mathbf{q}|=\sqrt{(q^1)^2+(q^2)^2+(q^3)^2},$$

therefore we get

$$N^\mu N_\mu(t_n+\tau,\mathbf{x}) = ((N^0)^2-(N^1)^2-(N^2)^2-(N^3)^2)(t_n+\tau,\mathbf{x})$$
$$> N^0(t_n+\tau,\mathbf{x})\left(N^0(t_n+\tau,\mathbf{x}) - \int_{\mathbb{R}^3}\frac{\sum_{k=1}^3 (q^k)^2}{|\mathbf{q}|^2} f_n\left(\mathbf{x}-\tau\frac{\mathbf{q}}{|\mathbf{q}|},\mathbf{q}\right)\mathrm{d}^3q\right)$$
$$= N^0(t_n+\tau,\mathbf{x})\left[N^0(t_n+\tau,\mathbf{x}) - \int_{\mathbb{R}^3} f_n\left(\mathbf{x}-\tau\frac{\mathbf{q}}{|\mathbf{q}|},\mathbf{q}\right)\mathrm{d}^3q\right] = 0.$$

Thus we have proved that $n(t_n+\tau,\mathbf{x}) = \sqrt{N^\mu N_\mu(t_n+\tau,\mathbf{x})} > 0$.

Now using the kinetic scheme $(4.1)_2$ and relation (2.16), we get

$$p(t_n+\tau,\mathbf{x}) = \frac{1}{3}e(t_n+\tau,\mathbf{x}) = \frac{1}{3}u_\mu u_\nu T^{\mu\nu}(t_n+\tau,\mathbf{x}) = \frac{1}{3}\int_{\mathbb{R}^3} q^\mu q^\nu f_n\left(\mathbf{x}-\tau\frac{\mathbf{q}}{|\mathbf{q}|},\mathbf{q}\right)\frac{\mathrm{d}^3q}{|\mathbf{q}|}u_\mu u_\nu$$
$$= \frac{1}{3}\int_{\mathbb{R}^3}\left(q^\mu u_\mu\right)^2 f_n\left(\mathbf{x}-\tau\frac{\mathbf{q}}{|\mathbf{q}|},\mathbf{q}\right)\frac{\mathrm{d}^3q}{|\mathbf{q}|} > 0.$$

Thus we conclude that $p(t_n+\tau,\mathbf{x}) > 0$. Also we know from $(4.1)_2$ that

$$T^{00}(t_n+\tau,\mathbf{x}) = \int_{\mathbb{R}^3}|\mathbf{q}| f_n\left(\mathbf{x}-\tau\frac{\mathbf{q}}{|\mathbf{q}|},\mathbf{q}\right)\mathrm{d}^3q > 0. \tag{4.14}$$

Now since our scheme is conservative, using (4.11), (4.14) and $|\mathbf{q}| = \sqrt{\sum_{k=1}^3 (q^k)^2}$, we have

$$||N^0(t_n+\tau,.)||_{L^1(R)} = \int_{\mathbb{R}^3}|N^0(t_n+\tau,\mathbf{x})|\mathrm{d}^3\mathbf{x} = \int_{\mathbb{R}^3} N^0(t_n+\tau,\mathbf{x})\mathrm{d}^3\mathbf{x} = \int_{\mathbb{R}^3} N^0(t_n,\mathbf{x})\mathrm{d}^3\mathbf{x}$$
$$= \int_{\mathbb{R}^3}|N^0(t_n,\mathbf{x})|\mathrm{d}^3\mathbf{x} = ||N^0(t_n,.)||_{L^1(R)}.$$

Similarly $||T^{00}(t_n+\tau,.)||_{L^1(R)} = \|T^{00}(t_n,.)\|_{L^1(R)}$. Now using (4.1) with $\mathbf{y} = \mathbf{x}-\tau\frac{\mathbf{q}}{|\mathbf{q}|}$ and Cauchy–Schwarz inequality (4.10) we get

$$||T^{0k}(t_n+\tau,.)||_{L^1(R)} = \int_{\mathbb{R}^3}\left|\int_{\mathbb{R}^3} q^k f_n(\mathbf{y},\mathbf{q})\frac{\mathrm{d}^3q}{|\mathbf{q}|}\right|\mathrm{d}^3\mathbf{x} = \int_{\mathbb{R}^3}\left|\int_{\mathbb{R}^3}\left(\sqrt{f_n}\right)\left(q^k\sqrt{f_n}\right)(\mathbf{y},\mathbf{q})\frac{\mathrm{d}^3q}{|\mathbf{q}|}\right|\mathrm{d}^3\mathbf{x}$$
$$< \left[\int_{\mathbb{R}^3}\left|\int_{\mathbb{R}^3} f_n(\mathbf{y},\mathbf{q})\frac{\mathrm{d}^3q}{|\mathbf{q}|}\right|\mathrm{d}^3\mathbf{x}\cdot\int_{\mathbb{R}^3}\left|\int_{\mathbb{R}^3}|\mathbf{q}|^2 f_n(\mathbf{y},\mathbf{q})\frac{\mathrm{d}^3q}{|\mathbf{q}|}\right|\mathrm{d}^3\mathbf{x}\right]^{1/2}$$
$$= \left(||n(t_n,.)||_{L^1(R)}||T^{00}(t_n,.)||_{L^1(R)}\right)^{1/2}.$$

This proves the L^1-stability of the scheme. □

5. First-order kinetic scheme in 1D

In the following we are looking for spatially one-dimensional solutions, which are nevertheless solutions to the full three-dimensional equations. We only consider solutions which depend on t and $x = x^1$ and satisfy $n = n(t,x)$, $\mathbf{u} = (u(t,x),0,0)$, $p = p(t,x)$. We will use the generally valid Equation $p = nT$ and go back to the full three-dimensional scheme.

In order to calculate the surface integrals (4.4) we introduce instead of the unit vector $\mathbf{w}$ the new variables $-1 \leqslant \xi \leqslant 1$ and $0 \leqq \varphi \leqq 2\pi$ by

$$w^1 = \xi, \quad w^2 = \sqrt{1-\xi^2}\sin\varphi, \quad w^3 = \sqrt{1-\xi^2}\cos\varphi \tag{5.1}$$

with the surface element $\mathrm{d}S(\mathbf{w}) = \mathrm{d}\xi\,\mathrm{d}\varphi$.

Note that the quantities n, T, u in the integrals (4.4) do not depend on the variable φ. This fact enables us to carry out the integration with respect to φ directly. Thus the twofold surface integral reduces to a simple ξ-integral. For abbreviation we introduce

$$\Phi(y,\xi) = \frac{1}{2}\frac{n(y)}{\left(\sqrt{1+u^2(y)} - \xi u(y)\right)^3}, \quad \Psi(y,\xi) = \frac{3}{2}\frac{(nT)(y)}{\left(\sqrt{1+u^2(y)} - \xi u(y)\right)^4}, \tag{5.2}$$

then the reduced integrals for the moments can be written as

$$N^0(t_n+\tau_M,x) = \int_{-1}^{1} \Phi(x-\tau_M\xi,\xi)\,\mathrm{d}\xi, \quad N^1(t_n+\tau_M,x) = \int_{-1}^{1} \xi\Phi(x-\tau_M\xi,\xi)\,\mathrm{d}\xi, \tag{5.3}$$

$$\begin{aligned} T^{00}(t_n+\tau_M,x) &= \int_{-1}^{1} \Psi(x-\tau_M\xi,\xi)\,\mathrm{d}\xi,\\ T^{01}(t_n+\tau_M,x) &= \int_{-1}^{1} \xi\Psi(x-\tau_M\xi)\,\mathrm{d}\xi,\\ T^{11}(t_n+\tau_M,x) &= \int_{-1}^{1} \xi^2\Psi(x-\tau_M\xi)\,\mathrm{d}\xi. \end{aligned} \tag{5.4}$$

In order to obtain the fields n, u and p we can use the one-dimensional form of (3.8) as

$$\begin{aligned} p(t_n+\tau_M,\mathbf{x}) &= \frac{1}{3}\left[-T^{00} + \sqrt{4(T^{00})^2 - 3(T^{01})^2}\right],\\ u(t_n+\tau_M,\mathbf{x}) &= \frac{T^{01}}{\sqrt{4p(t_n+\tau_M,\mathbf{x})\left[p(t_n+\tau_M,\mathbf{x}) + T^{00}\right]}},\\ n(t_n+\tau_M,\mathbf{x}) &= \frac{N^0}{\sqrt{1+u(t_n+\tau_M,\mathbf{x})^2}}. \end{aligned} \tag{5.5}$$

Here again $N^0 = N^0(t_n+\tau_M,x)$, $T^{00} = T^{00}(t_n+\tau_M,x)$ and $T^{01} = T^{01}(t_n+\tau_M,x)$ are given by the above kinetic scheme.

5.1. Numerical implementation of the scheme in 1D

Here we explain the numerical implementation of the one-dimensional kinetic scheme. However the procedure is similar for the multi-dimensional case.

- We start with the values of initial data $n(t_n,x)$, $u(t_n,x)$ and $T(t_n,x)$ at equidistant grid points.
- We specify the length L of the spatial cells, the number N_x of elements (intervals) in the spatial domain $0 \leqslant x \leqslant L$, the final time t_f of output and the number E_m of maximization times. For $i = 0,\ldots,N_x$, we introduce the nodes $x_i = i \cdot \frac{L}{N_x}$.
- The time step τ_M is calculated by $\tau_M = \frac{t_f}{E_m}$. The step in the spatial domain is $\Delta x = L/N_x$.
- Our aim is to calculate the moments (5.3) and (5.4). These moments are then used to update the fields n, u and T.

- Since we only know the values of the fields at the nodal points, the free-flight fields in the integrands of (5.3) and (5.4) must be calculated from the knowledge of the nodal values at the points x_i. Here we use linear interpolation between two subsequent nodal points x_i and x_{i+1}. We use the following interpolation formula:

$$\begin{aligned}\phi(x_j - \xi\tau, \xi) &= (1-\eta)\phi(x_i, \xi) + \eta\phi(x_{i+1}, \xi),\\ \psi(x_j - \xi\tau, \xi) &= (1-\eta)\psi(x_i, \xi) + \eta\psi(x_{i+1}, \xi),\end{aligned} \tag{5.6}$$

  where $x_j - \xi\tau = x_i + \eta(x_{i+1} - x_i)$ for $0 \leqslant \eta \leqslant 1$. Here $\phi(x_i, \xi)$ and $\psi(x_i, \xi)$ are the phase densities given by (5.2). The relation between x_i, x_j and η is shown in Fig. 1.
- The ξ-integration in the moment integrals is performed with the composite trapezoidal rule.
- The values of the fields n, u and T are calculated by using the relations (5.5). These fields are used in order to initialize the scheme for the next time step.

5.2. Application of boundary conditions

Here we generalize the above numerical kinetic scheme in order to include boundaries. We are restricting ourselves to one space dimension, however the procedure is analogous for the multi-dimensional case.

It is possible that a point $y = x - \xi\tau$ is outside the computational domain $0 \leqslant x \leqslant L$, i.e., the fluid particle has then crossed the domain boundaries during free-flight. Consequently, a boundary strategy is required to find $f_n(y, \xi)$ so that physically meaningful desired boundary conditions are satisfied.

5.2.1. Reflecting boundary conditions

In Fig. 2 a single gas particle trajectory is shown. We consider the lower boundary as a solid wall, therefore the particles having negative velocity will reach the wall. The particle starts from a position x_* with negative microscopic velocity and reach the lower boundary in time τ_1. The particle then reflects with positive velocity and reaches the position x in time τ_2. Since the reflection from the lower adiabatic wall is

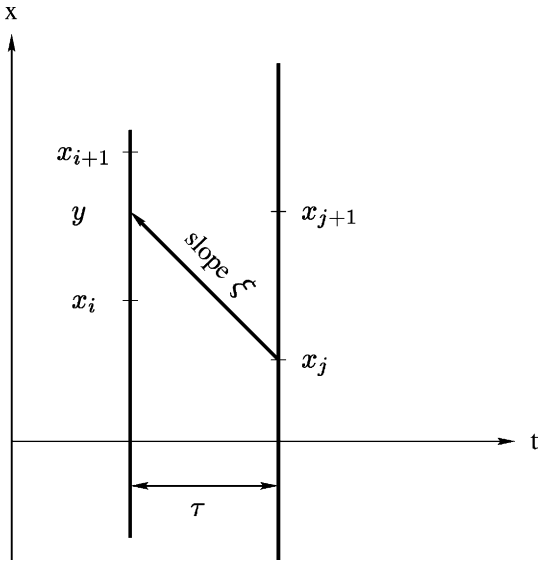

Fig. 1. Interpolation of $y = x_j - \xi\tau$ at the grid points x_i and x_{i+1}.

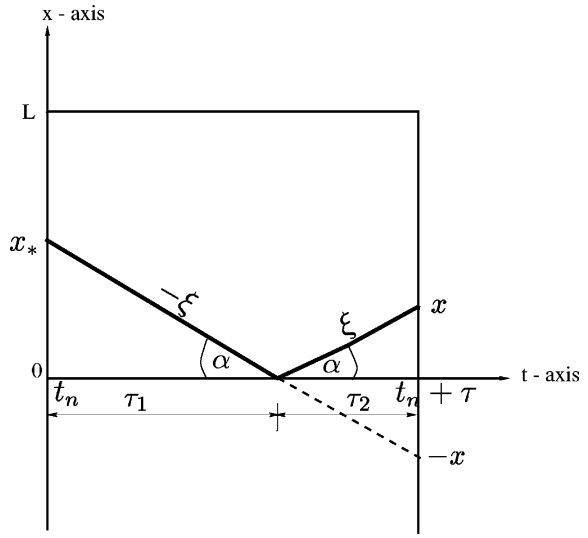

Fig. 2. Trajectory of a single gas particle.

elastic, therefore particle incident and reflected angles are the same. Now using Fig. 2 we get the following relations:

$$x = \tau_2\xi, \quad x_* = -\tau_1\xi, \quad \tau_1 + \tau_2 = \tau. \tag{5.7}$$

Subtracting $(5.7)_{1,2}$ and using $(5.7)_3$ we get $x_* = |x - \tau\xi| \geqslant 0$.

Therefore in case of lower adiabatic boundary we replace $\phi(x - \tau\xi, \xi)$ and $\psi(x - \tau\xi, \xi)$ in the kinetic scheme (5.3) and (5.4) by $\phi(|x - \tau\xi|, \xi_*)$ and $\psi(|x - \tau\xi|, \xi_*)$ for $\xi_* = -\xi$.

Similarly if we consider the boundary $x = L$ as adiabatic wall then only those particles will reach to the boundary which have positive microscopic velocity ξ. Let $\Delta = y - L$ then the reflecting boundary conditions will be $x_* = L - \Delta$ and $\xi_* = -\xi$. Thus we will replace $\phi(x - \tau\xi, \xi)$ and $\phi(x - \tau\xi, \xi)$ in the kinetic scheme (5.3) and (5.4) by $\phi(x_*, \xi_*)$ and $\psi(x_*, \xi_*)$.

5.2.2. Absorbing boundary conditions

When the fluid particle crosses the lower boundary as shown by dashed line in Fig. 2, i.e., $y = x - \xi\tau < 0$, then we replace $\phi(x - \tau\xi, \xi)$ and $\phi(x - \tau\xi, \xi)$ in the kinetic scheme (5.3) and (5.4) by $\phi(|x - \tau\xi|, \xi)$ and $\psi(|x - \tau\xi|, \xi)$. Similarly if $y = x - \xi\tau > L$, i.e., fluid particles have acrossed the upper boundary then we take $x_* = L - \Delta$ where $\Delta = y - L$ and replace $\phi(x - \tau\xi, \xi)$ and $\phi(x - \tau\xi, \xi)$ in the kinetic scheme (5.3) and (5.4) by $\phi(x_*, \xi)$ and $\psi(x_*, \xi)$.

5.2.3. Inflow boundary conditions

Let ρ_l, v_l, T_l and ρ_u, v_u, T_u be the given values of the fields at lower or upper boundaries, respectively. When the fluid particle is at the lower boundary, i.e., $y = x - \xi\tau \leqslant 0$, then we calculate

$$f_n(y, \xi) = f_n(\rho_\mathrm{l}, v_\mathrm{l}, T_\mathrm{l}, \xi).$$

Similarly if $y = x - \xi\tau \geqslant L$, then we calculate

$$f_n(y, \xi) = f_n(n_\mathrm{u}, v_\mathrm{u}, T_\mathrm{u}, \xi).$$

6. Second-order one-dimensional kinetic scheme

Here we extend our one-dimensional kinetic scheme [24] to second order. We will use the approach of Deshpande [8] which he has used in order to obtain second-order accuracy in a one-dimensional kinetic scheme for the non-relativistic Euler equations. There are two steps in order to get second-order accuracy in time. In the first step we will proceed to achieve second-order accuracy in time, while the second step is to achieve second-order accuracy in space. There are two approaches to achieve second-order accuracy in time and both approaches lead to the same result. We will present both approaches in our study.

The first-order kinetic schemes described in the previous sections suffer from the major disadvantage that the numerical diffusion is proportional to the time step. From the physical point of view, such a result is only to be expected because the fluid particles in the above kinetic schemes are allowed to move over the time step τ_M before they undergo collisions. The distance traveled between collisions is thus proportional to τ_M. From the kinetic theory it then follows that the mean free path, and hence the viscosity, will be of the order τ_M. This is a very large amount of viscosity, as the results shown later will verify. Therefore, a modifications in the above kinetic schemes is required that will ensure that the method has a high-order accuracy. We will show how it is possible to achieve second-order accuracy.

6.1. First approach: second-order accuracy in time

First we aim for second-order accuracy in time. For this purpose it will be sufficient to consider the zero components N^0, T^{01} and T^{00}. In the following calculations we only follow the component N^0 because the procedure for T^{01} and T^{00} is similar. The second-order accurate Taylor expansions of $N^0(t_n+\tau_M,x)$ is

$$N^0(t_n+\tau_M,x) = N^0(t_n,x) + \tau_M \frac{\partial N^0}{\partial t}(t_n,x) + \frac{1}{2}\tau_M^2 \frac{\partial^2 N^0}{\partial t^2}(t_n,x) + \mathrm{O}(\tau_M^3). \tag{6.1}$$

This expansions contain the first- and second-order time derivatives of N^0. Similar expansion can also be obtained for $T^{01}(t_n+\tau_M,x)$ and $T^{00}(t_n+\tau_M,x)$. The first-order time derivatives can be replaced in terms of the first-order space derivatives by using the Euler equations (3.9). To replace the second-order time derivatives in terms of space derivatives requires detailed manipulations. Using Eqs. (3.9) and (3.10) in (6.1) we get

$$N^0(t_n+\tau_M,x) = N^0(t_n,x) - \tau_M \frac{\partial N^1}{\partial x}(t_n,x) - \frac{1}{2}\tau_M^2 \frac{\partial}{\partial x}\left(\frac{\partial N^1}{\partial t}(t_n,x)\right) + \mathrm{O}(\tau_M^3). \tag{6.2}$$

Our main goal is to compare the second-order accurate Taylor expansion (6.2) for $N^0(t_n+\tau_M,x)$ and similarly for $T^{01}(t_n+\tau_M,x)$ and $T^{00}(t_n+\tau_M,x)$ with the kinetic scheme (5.3) and (5.4) after expanding the free-flight phase densities up to $\mathrm{O}(\tau_M^3)$. This comparison will give us the terms which are missing in the first-order kinetic schemes, the so-called antidiffusive terms. The addition of these terms will lead to the second-order accuracy in time of the first-order kinetic scheme.

In order to compare Eqs. (6.2) with the kinetic scheme solutions (5.3) and (5.4), we take a second-order accurate Taylor expansion of the reduced free-flight phase densities $\phi(x-\tau_M\xi,\xi)$ and $\psi(x-\tau_M\xi,\xi)$ given in (5.2). Here again we only follow the expansion of $\phi(x-\tau_M\xi,\xi)$ since the procedure is similar for $\psi(x-\tau_M\xi,\xi)$, we get

$$\phi(x-\tau_M\xi,\xi) = \phi(t_n,x,\xi) - \xi\tau_M \frac{\partial \phi}{\partial x}(t_n,x,\xi) + \frac{\xi^2\tau_M^2}{2}\frac{\partial^2\phi}{\partial x^2}(t_n,x,\xi) + \mathrm{O}(\tau_M^3). \tag{6.3}$$

Integrating (6.3) we get for $\phi = \phi(t_n,x,\xi)$,

$$\int_{-1}^{1}\phi(x-\tau_M\xi,\xi)\,\mathrm{d}\xi = \int_{-1}^{1}\phi\,\mathrm{d}\xi - \tau_M\frac{\partial}{\partial x}\int_{-1}^{1}\xi\phi\,\mathrm{d}\xi + \frac{1}{2}\tau_M^2\frac{\partial}{\partial x}\left(\frac{\partial}{\partial x}\int_{-1}^{1}\xi^2\phi\,\mathrm{d}\xi\right) + \mathrm{O}(\tau_M^3). \tag{6.4}$$

The reduced equilibrium phase density $\phi(t_n, x, \xi)$ satisfy the following relation:

$$N^0(t_n, x) = \int_{-1}^{1} \phi(t_n, x, \xi)\, \mathrm{d}\xi. \tag{6.5}$$

Similar relations also exists in case of the reduced phase density $\psi(t_n, x, \xi)$. Using the relations (6.5) in (6.4) we finally get

$$\int_{-1}^{1} \phi(x - \tau_M \xi, \xi)\, \mathrm{d}\xi = N^0(t_n, x) - \tau_M \frac{\partial N^1}{\partial x}(t_n, x) + \frac{1}{2}\tau_M^2 \frac{\partial}{\partial x}\left(\frac{\partial}{\partial x}\int_{-1}^{1} \xi^2 \phi\, \mathrm{d}\xi\right) + \mathrm{O}(\tau_M^3). \tag{6.6}$$

Eqs. (6.6) is the solution coming from the first-order kinetic schemes (5.3) and (5.4) when we expand the free-flight phase density up to $\mathrm{O}(\tau_M^3)$. Similar relations can also be obtained in case of the phase density $\psi(x - \tau_M \xi, \xi)$ by repeating the above procedure.

Now we can rewrite the second-order accurate solutions (6.2) in the following form by adding and subtracting appropriate order τ_M^2 term that appeared in (6.6):

$$\begin{aligned} N^0(t_n + \tau_M, x) = {} & N^0(t_n, x) - \tau_M \frac{\partial N^1}{\partial x}(t_n, x) + \frac{1}{2}\tau_M^2 \frac{\partial}{\partial x}\left(\frac{\partial}{\partial x}\int_{-1}^{1} \xi^2 \phi\, \mathrm{d}\xi\right) \\ & - \frac{1}{2}\tau_M^2 \frac{\partial}{\partial x}\left(\frac{\partial N^1}{\partial t}(t_n, x) + \frac{\partial}{\partial x}\int_{-1}^{1} \xi^2 \phi\, \mathrm{d}\xi\right) + \mathrm{O}(\tau_M^3). \end{aligned} \tag{6.7}$$

Now using (6.6) in (6.7) and repeating the above steps for $T^{01}(t_n + \tau_M, x)$ and $T^{00}(t_n + \tau_M, x)$ we finally get

$$\begin{aligned} N^0(t_n + \tau_M, x) &= \int_{-1}^{1} \phi(x - \tau_M, \xi)\, \mathrm{d}\xi - \frac{1}{2}\tau_M^2 \frac{\partial}{\partial x}\left(\frac{\partial N^1}{\partial t}(t_n, x) + \frac{\partial}{\partial x}\int_{-1}^{1} \xi^2 \phi\, \mathrm{d}\xi\right) + \mathrm{O}(\tau_M^3), \\ T^{01}(t_n + \tau_M, x) &= \int_{-1}^{1} \xi \psi(x - \tau_M, \xi)\, \mathrm{d}\xi - \frac{1}{2}\tau_M^2 \frac{\partial}{\partial x}\left(\frac{\partial T^{11}}{\partial t}(t_n, x) + \frac{\partial}{\partial x}\int_{-1}^{1} \xi^3 \psi\, \mathrm{d}\xi\right) + \mathrm{O}(\tau_M^3), \\ T^{00}(t_n + \tau_M, x) &= \int_{-1}^{1} \psi(x - \tau_M, \xi)\, \mathrm{d}\xi + \mathrm{O}(\tau_M^3). \end{aligned} \tag{6.8}$$

Using Appendix A we can simplify the terms of order τ_M^2 in $(6.8)_{1,2}$ in order to get

$$\begin{aligned} N^0(t_n + \tau_M, x) &= \int_{-1}^{1} \phi(x - \tau_M \xi, \xi)\, \mathrm{d}\xi + \frac{1}{2}\tau_M^2 \frac{\partial}{\partial x} g(n, u, p) + \mathrm{O}(\tau_M^3), \\ T^{01}(t_n + \tau_M, x) &= \int_{-1}^{1} \xi \psi(x - \tau_M \xi, \xi)\, \mathrm{d}\xi + \frac{1}{2}\tau_M^2 \frac{\partial}{\partial x} h(u, p) + \mathrm{O}(\tau_M^3), \\ T^{00}(t_n + \tau_M, x) &= \int_{-1}^{1} \psi(x - \tau_M \xi, \xi)\, \mathrm{d}\xi + \mathrm{O}(\tau_M^3), \end{aligned} \tag{6.9}$$

where

$$\begin{aligned} g(n, u, p) = {} & \left(-\frac{(1 + u^2)^{-1/2}}{u^2} + \frac{1}{u^3}\ \mathrm{arcsinh}(u)\right)\frac{\partial n}{\partial x} - \frac{3n(1 + u^2)^{-1/2}}{4p(3 + 2u^2)}\frac{\partial p}{\partial x} \\ & + \left(\frac{9n\sqrt{1 + u^2}}{u^3(3 + 2u^2)} - \frac{3n}{u^4}\ \mathrm{arcsinh}(u)\right)\frac{\partial u}{\partial x}, \\ h(u, p) = {} & \left(\frac{9\sqrt{1 + u^2}}{u^4(3 + 2u^2)} + \frac{3\ \mathrm{arcsinh}(-u)}{u^5}\right)\left(u\frac{\partial p}{\partial x} - 4p\frac{\partial u}{\partial x}\right). \end{aligned} \tag{6.10}$$

On the right-hand sides of Eqs. $(6.9)_{1,2}$ the first terms are from the old kinetic scheme, while the second terms are the antidiffusive terms which must be added to N^0 and T^{01} for the second-order accuracy. While the energy density T^{00} is already second-order accurate in time. In the non-relativistic case Deshpande [8] observed that the particle density coming from the first-order kinetic scheme was already second-order accurate in time, but in the first-order relativistic kinetic scheme we found that the energy density is second-order accurate in time. This is due to the fact that in the non-relativistic Euler equations case the flux of the continuity equation is equal to the conserved momentum variable, while in the relativistic Euler equations case the flux in the total energy equation is equal to the conserved momentum variable.

6.2. Second approach: second-order accuracy in time

Since the free-flight phase density is very far from equilibrium, the reduced phase densities $\phi(t,x,\xi)$ and $\psi(t,x,\xi)$ given by (5.2) do not satisfy the reduced free-flight transport equation, i.e.,

$$\frac{\partial\phi}{\partial t}+\xi\frac{\partial\phi}{\partial x}\neq 0,\quad \frac{\partial\psi}{\partial t}+\xi\frac{\partial\psi}{\partial x}\neq 0. \tag{6.11}$$

In fact from (5.2) we have

$$\frac{\partial\phi}{\partial t}+\xi\frac{\partial\phi}{\partial x}=\left(\frac{\partial n}{\partial t}+\xi\frac{\partial n}{\partial x}\right)\frac{\partial\phi}{\partial n}+\left(\frac{\partial u}{\partial t}+\xi\frac{\partial u}{\partial x}\right)\frac{\partial\phi}{\partial u}, \tag{6.12}$$

$$\frac{\partial\psi}{\partial t}+\xi\frac{\partial\psi}{\partial x}=\left(\frac{\partial p}{\partial t}+\xi\frac{\partial p}{\partial x}\right)\frac{\partial\psi}{\partial p}+\left(\frac{\partial u}{\partial t}+\xi\frac{\partial u}{\partial x}\right)\frac{\partial\psi}{\partial u}. \tag{6.13}$$

The right-hand sides of (6.12) and (6.13) are very characteristic of the Chapman–Enskog (CE) non-relativistic theory and the method of Ohwada [29]. Using Appendix A we can replace the time derivatives of n, u and p in Eqs. (6.13) and (6.13) in terms of the space derivatives. We obtain

$$\frac{\partial\phi}{\partial t}+\xi\frac{\partial\phi}{\partial x}=Q_{\mathrm{CE}}\phi, \tag{6.14}$$

$$\frac{\partial\psi}{\partial t}+\xi\frac{\partial\psi}{\partial x}=M_{\mathrm{CE}}\psi, \tag{6.15}$$

where Q_{CE} and M_{CE} are polynomials given by

$$Q_{\mathrm{CE}}=Q_1\frac{\partial n}{\partial x}+Q_2\frac{\partial p}{\partial x}+Q_3\frac{\partial u}{\partial x}, \tag{6.16}$$

$$M_{\mathrm{CE}}=M_1\frac{\partial p}{\partial x}+M_2\frac{\partial u}{\partial x}, \tag{6.17}$$

with

$$\begin{aligned} Q_1&=\frac{\xi\sqrt{1+u^2}-u}{n\sqrt{1+u^2}},\quad Q_2=\frac{3\left(4u\sqrt{1+u^2}-4u^2\xi-3\xi\right)}{4p\sqrt{1+u^2}(3+2u^2)(\sqrt{1+u^2}-\xi u)},\\ Q_3&=3\left(\frac{\xi^2\sqrt{1+u^2}(3+2u^2)+2u^2(\sqrt{1+u^2}-\xi u)-\sqrt{1+u^2}(1+2\xi u\sqrt{1+u^2})-2\xi u}{\sqrt{1+u^2}(3+2u^2)(\sqrt{1+u^2}-\xi u)}\right), \end{aligned} \tag{6.18}$$

and

$$M_1 = \frac{u(1-3\xi^2) + 2u^2(2\sqrt{1+u^2}\xi - \xi^2 u - u)}{p(3+2u^2)(\sqrt{1+u^2} - \xi u)}, \quad M_2 = \frac{4}{3}Q_3. \tag{6.19}$$

The polynomials Q_{CE} and Q_{CE} have interesting properties, i.e.,

$$\int_{-1}^{1} Q_{\mathrm{CE}}\phi \,\mathrm{d}\xi = 0, \quad \int_{-1}^{1} M_{\mathrm{CE}}\psi \,\mathrm{d}\xi = 0, \quad \int_{-1}^{1} \xi M_{\mathrm{CE}}\psi \,\mathrm{d}\xi = 0. \tag{6.20}$$

These properties follow from the integration of (6.14) and (6.15) and the fact that the moments satisfy conservation laws. Furthermore, one can directly check these properties by a simple ξ-integration in mathematics packages like, Maple or Mathematica. We will see at the end that these properties are also important for the conservativity of the second-order kinetic scheme. We are now ready to construct the second-order accurate kinetic scheme which was also obtained in the *first approach*. In the following we give the details of the procedure for $N^0(t_n + \tau_M, x)$, because it follow the similar steps for $T^{01}(t_n + \tau_M, x)$ and $T^{00}(t_n + \tau_M, x)$. Using the Taylor expansion we have

$$N^0(t_n + \tau_M, x) = \int_{-1}^{1} \phi(t_n + \tau_M, x, \xi)\,\mathrm{d}\xi = \int_{-1}^{1} \left(\phi + \tau_M \frac{\partial \phi}{\partial t} + \frac{1}{2}\tau_M^2 \frac{\partial^2 \phi}{\partial t^2}\right) \mathrm{d}\xi + \mathrm{O}(\tau_M^3), \tag{6.21}$$

where $\phi = \phi(t_n, x, \xi)$. As stated before the equilibrium phase densities ϕ and ψ do not satisfy the free-flight equation. But on the other hand they satisfy the moment equations of the free-flight equation which are infact the Euler equations, for example,

$$\int_{-1}^{1} \frac{\partial \phi}{\partial t}\,\mathrm{d}\xi + \int_{-1}^{1} \xi \frac{\partial \phi}{\partial x}\,\mathrm{d}\xi = 0, \tag{6.22}$$

is the continuity equation of the Euler equations (3.9). Similarly energy and momentum equations can be obtained from the moment equations of ψ. Therefore, in order to replace the first-order time derivative of ϕ in above expression we use (6.21) and (6.22), we get

$$N^0(t_n + \tau_M, x) = \int_{-1}^{1} \left(\phi - \tau_M \xi \frac{\partial \phi}{\partial x} + \frac{1}{2}\tau_M^2 \frac{\partial^2 \phi}{\partial t^2}\right) \mathrm{d}\xi + \mathrm{O}(\tau_M^3). \tag{6.23}$$

Using the relation (6.14), we obtain

$$\frac{\partial^2 \phi}{\partial t^2} = -\xi \frac{\partial}{\partial x}\left(\frac{\partial \phi}{\partial t}\right) + \frac{\partial}{\partial t}(Q_{\mathrm{CE}}\phi) = \xi^2 \frac{\partial^2 \phi}{\partial x^2} - \xi \frac{\partial}{\partial x}(Q_{\mathrm{CE}}\phi) + \frac{\partial}{\partial t}(Q_{\mathrm{CE}}\phi). \tag{6.24}$$

Substituting the above expression for the second-order derivatives of ϕ in (6.23) we get after using (6.3) for $y = x - \tau_M \xi$,

$$N^0(t_n + \tau_M, x) = \int_{-1}^{1} \phi(y, \xi)\,\mathrm{d}\xi - \frac{\tau_M^2}{2}\left(\int_{-1}^{1} \xi \frac{\partial}{\partial x}(Q_{\mathrm{CE}}\phi)\,\mathrm{d}\xi - \frac{\partial}{\partial t}\int_{-1}^{1} Q_{\mathrm{CE}}\phi \,\mathrm{d}\xi\right) + \mathrm{O}(\tau_M^3).$$

The last terms in the $\mathrm{O}(\tau_M^3)$ part of the above equation are zero due to the properties (6.20) of $Q_{\mathrm{CE}}\phi$. After repeating the above steps for other components $T^{01}(t_n + \tau_M, x)$ and $T^{00}(t_n + \tau_M, x)$ we finally get

$$N^0(t_n + \tau_M, x) = \int_{-1}^{1} \phi(y, \xi)\,\mathrm{d}\xi - \frac{1}{2}\tau_M^2 \int_{-1}^{1} \xi \frac{\partial}{\partial x}(Q_{\mathrm{CE}}\phi(t_n, x, \xi))\,\mathrm{d}\xi + \mathrm{O}(\tau_M^3), \tag{6.25}$$

$$T^{01}(t_n+\tau_M,x)=\int_{-1}^{1}\xi\psi(y,\xi)\,\mathrm{d}\xi-\frac{1}{2}\tau_M^2\int_{-1}^{1}\xi^2\frac{\partial}{\partial x}(Q_{\mathrm{CE}}\phi(t_n,x,\xi))\,\mathrm{d}\xi+\mathrm{O}(\tau_M^3),$$
$$T^{00}(t_n+\tau_M,x)=\int_{-1}^{1}\psi(y,\xi)\,\mathrm{d}\xi+\mathrm{O}(\tau_M^3), \tag{6.26}$$

which shows that in addition to the $\phi(y,\xi)$ and $\psi(y,\xi)$ terms we have one more term in the first two equations containing the polynomials Q_{CE} and M_{CE}. Hence the reduced Jüttner distributions ϕ and ψ alone will not yield a second-order accurate kinetic scheme for particle density and momentum, however the total energy T^{00} is already second-order accurate in time. Note that if we evaluate the integrals of the second terms in (6.25) and $(6.26)_1$, we get the same correction terms g and h as given in (6.9). In order to obtain (6.9) one can simply integrate the coefficients of τ_M^2 in above equation using Mathematica or Maple. Let us define

$$\phi_{\mathrm{CE}}(y,\xi)=\phi\Big(1+\frac{\tau_M}{2}Q_{\mathrm{CE}}\Big)(y,\xi),\quad \psi_{\mathrm{CE}}(y,\xi)=\psi\Big(1+\frac{\tau_M}{2}M_{\mathrm{CE}}\Big)(y,\xi). \tag{6.27}$$

We can recast (6.25) and (6.26) as

$$N^0(t_n+\tau_M,x)=\int_{-1}^{1}\phi_{\mathrm{CE}}(x-\tau_M\xi,\xi)\,\mathrm{d}\xi+\mathrm{O}(\tau_M^3),$$
$$T^{01}(t_n+\tau_M,x)=\int_{-1}^{1}\xi\psi_{\mathrm{CE}}(x-\tau_M\xi,\xi)\,\mathrm{d}\xi+\mathrm{O}(\tau_M^3), \tag{6.28}$$
$$T^{00}(t_n+\tau_M,x)=\int_{-1}^{1}\psi_{\mathrm{CE}}(x-\tau_M\xi,\xi)\,\mathrm{d}\xi+\mathrm{O}(\tau_M^3).$$

Due to the properties (6.20) of $Q_{\mathrm{CE}}\phi$ and $M_{\mathrm{CE}}\psi$ we can see that the zero quantities N^0, T^{01} and T^{00} are identical within the truncation error, i.e.

$$\int_{-1}^{1}(\phi_{\mathrm{CE}}-\phi)\,\mathrm{d}\xi=0,\quad \int_{-1}^{1}\xi(\psi_{\mathrm{CE}}-\psi)\,\mathrm{d}\xi=0,\quad \int_{-1}^{1}(\psi_{\mathrm{CE}}-\psi)\,\mathrm{d}\xi=0.$$

These conditions also can be regarded as conservation conditions, for more details see Deshpande [8] in the non-relativistic case.

Several important features of the above second-order accurate in time kinetic scheme are worth noting. Eqs. (6.28), containing different distribution functions, have been obtained from Eqs. (6.9) or (6.25). As stated before the right-hand sides of Eqs. $(6.9)_{1,2}$ and $(6.25)_{1,2}$ contain two terms. The first terms, which are moments of the free-flight phase densities $\phi(x-\xi\tau_M,\xi)$ and $\phi(x-\xi\tau_M,\xi)$, are upwind in character. The second terms cannot be expressed as moments of $\phi(x-\tau_M\xi,\xi)$ and $\psi(x-\tau_M\xi,\xi)$ and are antidiffusive. The antidiffusive terms may be absorbed in the upwind term only if the distribution function is not the relativistic Maxwellian, i.e., Jüttner distribution. Eqs. (6.28) are an upwind version of a second-order accurate solution in which the perturbed relativistic Maxwellian distributions are employed.

6.3. Second-order accuracy in space

Another important point about Eqs. (6.28) is that, $\phi_{\mathrm{CE}}(x-\xi\tau_M,\xi)$ and $\phi_{\mathrm{CE}}(x-\xi\tau_M,\xi)$ need to be evaluated at various values of ξ. Hence, as noted before, some kind of interpolation scheme is required. This scheme must be second-order accurate in space and should not yield non-negative interpolated values, and should satisfy the TVD property. A procedure is given below.

Let ϕ_{CE} and ψ_{CE} be given at mesh points. Also let the mesh point i corresponding to point j be such that

$$x_j-\xi\tau_M=x_i+\eta\Delta x,\quad 0\leqslant\eta\leqslant 1.$$

The relation between x_j and x_i and η is given in Fig. 1. The functions $\phi_{\mathrm{CE}}(x_j - \xi\tau_M, \xi) = \phi_{\mathrm{CE}}(x_i + \eta\Delta x, \xi)$ and $\psi_{\mathrm{CE}}(x_j - \xi\tau_M, \xi) = \psi_{\mathrm{CE}}(x_i + \eta\Delta x, \xi)$ then depends on the neighbouring mesh points $i \pm 1$. Therefore the second-order interpolation for any function f will be

$$f(x_i + \eta\Delta x, \xi) = f_i + \frac{\eta}{2}(f_{i+1} - f_{i-1}) + \frac{\eta^2}{2}(f_{i+1} - 2f_i + f_{i-1}), \tag{6.29}$$

where f_i can be $\phi_{\mathrm{CE}}(t_n, x_i, \xi)$ or $\psi_{\mathrm{CE}}(t_n, x_i, \xi)$. In order to suppress oscillations in the numerical results we use the min-mod nonlinear limiters [18,31,33] on the numerical derivatives appearing in the antidiffusive terms Q_{CE} and M_{CE} given in (6.16) and (6.17). These min-mod nonlinear limiters also ensure the positivity of the phase densities ϕ_{CE} and ψ_{CE}.

As pointed out by Deshpande [8], the expression (6.29) does not automatically ensure positivity of $f(x_i + \eta\Delta x, \xi)$ even if f_{i-1}, f_i and f_{i+1} are assumed to be positive. This is particularly true for calculations near shocks. With the method of Chakravarthy and Osher [2] limiting the contribution of the second difference, it is possible to devise an interpolation scheme that satisfies the TVD condition and guarantee the positivity of $\phi_{\mathrm{CE}}(x_i + \eta\Delta x, \xi)$ and $\psi_{\mathrm{CE}}(x_i + \eta\Delta x, \xi)$, see [8]. The second-order accurate Taylor expansion (6.29) can be rewritten as

$$\begin{aligned} f(x_i + \eta\Delta x, \xi) &= f_i + \frac{\eta}{2}(f_{i+1} - f_i + f_i - f_{i-1}) + \frac{\eta^2}{2}(f_{i+1} - f_i + f_{i-1} - f_i) \\ &= f_i + (f_{i+1} - f_i)\left[\frac{\eta(1+\eta)}{2} + \frac{\eta(1-\eta)}{2} r_{\mathrm{D}}\right], \end{aligned} \tag{6.30}$$

where

$$r_{\mathrm{D}} = \frac{\text{Backward difference}}{\text{Forward difference}} = \frac{f_i - f_{i-1}}{f_{i+1} - f_i}.$$

In smooth regions

$$f_{i\pm1} = f_i \pm \Delta x f_i' + \frac{(\Delta x)^2}{2} f_i'' + \mathrm{O}(\Delta x^3), \tag{6.31}$$

then

$$\begin{aligned} \frac{f_i - f_{i-1}}{\Delta x f_i'} &= 1 - \frac{\Delta x}{2}\frac{f_i''}{f_i'} + \mathrm{O}(\Delta x^2), \\ \frac{f_{i+1} - f_i}{\Delta x f_i'} &= 1 + \frac{\Delta x}{2}\frac{f_i''}{f_i'} + \mathrm{O}(\Delta x^2). \end{aligned} \tag{6.32}$$

This implies

$$\begin{aligned} r_{\mathrm{D}} = \frac{f_i - f_{i-1}}{f_{i+1} - f_i} &= \left(1 - \frac{\Delta x}{2}\frac{f_i''}{f_i'} + \mathrm{O}(\Delta x^2)\right)\left(1 + \frac{\Delta x}{2}\frac{f_i''}{f_i'} + \mathrm{O}(\Delta x^2)\right)^{-1}, \\ &= \left(1 - \frac{\Delta x}{2}\frac{f_i''}{f_i'} + \mathrm{O}(\Delta x^2)\right)\left(1 - \frac{\Delta x}{2}\frac{f_i''}{f_i'} + \mathrm{O}(\Delta x^2)\right). \end{aligned} \tag{6.33}$$

Hence we finally get

$$r_{\mathrm{D}} = 1 - \Delta x \frac{f_i''}{f_i'} + \mathrm{O}(\Delta x^2), \tag{6.34}$$

and thus r_D remains close to unity. In flow regions near shocks or contact surfaces, r_D can wildly vary and some limiting criterion is required to preserve the TVD condition. The key to satisfy the TVD condition lies in requiring

$$0 \leqslant \frac{\eta(1+\eta)}{2} + \frac{\eta(1-\eta)}{2} r_D \leqslant 1. \tag{6.35}$$

Two cases arise, namely, $r_D \geqslant 0$ and $r_D \leqslant 0$. If we consider the case of $r_D \geqslant 0$, the condition in Eq. (6.35) is satisfied if

$$r_D \leqslant 1 + \frac{2}{\eta}. \tag{6.36}$$

As $0 \leqslant \eta \leqslant 1$, the right-hand side of the above inequality has minimum value of 3. One way of satisfying Eq. (6.36) is to limit the value of r_D to 3 when $r_D \geqslant 0$. For the case when $r_D \leqslant 0$, the condition in Eq. (6.35) is satisfied if

$$\frac{\eta(1+\eta)}{2} + \frac{\eta(1-\eta)}{2} r_D = \frac{\eta(1+\eta)}{2} - \frac{\eta(1-\eta)}{2} |r_D| \geqslant 0, \tag{6.37}$$

or equivalently, if

$$|r_D| \leqslant \frac{1+\eta}{1-\eta}. \tag{6.38}$$

Thus, by limiting the relative values of the forward and backward differences and taking $r_D = 1$ outside these limits, we find the interpolation formula in Eq. (6.30) yields not only positive values of $f(x_i + \eta\Delta x, \xi)$ but also satisfies the TVD condition. As mentioned before the basic input to Eq. (6.30) is the set of positive values of f_i at all mesh points.

From the analysis in this section it has become clear that the second-order accurate kinetic scheme requires the use of distribution functions ϕ_{CE} and ψ_{CE} given in Eq. (6.27), as well as second-order accurate interpolation scheme. The extension of this kinetic scheme to two-dimensional case is analogous.

Remark. Due to the presence of Q_{CE} and M_{CE}, the distribution functions ϕ_{CE} and ψ_{CE} given in (6.27) not only depend on the local values of the field variables but also depend on their neighbouring values as well. The support of ϕ_{CE} and ψ_{CE} is thus more than that of local phase densities ϕ and ψ used in the first-order kinetic scheme.

7. Numerical case studies

In the following we present numerical test cases for the solution of the ultra-relativistic Euler equations. For the comparison we use exact Riemann solution, upwind [16] and central schemes of Nessayahu and Tadmor [28]. The CFL condition in the ultra-relativistic case is very simple which is $\Delta t = \Delta x/2$. This CFL condition comes out automatically due to the structure of light cones, since every signal speed is bounded by the velocity of light. In the following computations we have used the above CFL condition for the upwind and central schemes, while 100 maximizations times were used for our kinetic scheme.

Problem 1. Shock tube problem I

The initial data are

$$(n,u,p) = \begin{cases} (5.0, 0.0, 10.0) & \text{if } x < 0.5, \\ (1.0, 0.0, 0.5) & \text{if } x \geqslant 0.5. \end{cases}$$

The spatial domain is taken as $[0,1]$ with 400 mesh elements and the final time is $t = 0.5$. This problem involves the formation of an intermediate state bounded by a shock wave propagating to the right and a transonic rarefaction wave propagating to the left. The fluid in the intermediate state moves at a mildly relativistic speed ($v = 0.58c$) to the right. Flow particles accumulate in a dense shell behind the shock wave compressing the fluid and heating it. The fluid is extremely relativistic from a thermodynamic point of view, but only mildly relativistic dynamically. Figs. $(3)_{1,2}$ and $(4)_{1,2}$ show the particle density n, fluid velocity $v = u/\sqrt{1+u^2}$ and pressure p. Figs. $(3)_{3,4}$ and $(4)_{3,4}$ show the same results with zooming in order to easily compare the schemes.

Problem 2. Shock tube problem II

The initial data are

$$(n,u,p) = \begin{cases} (1.0, 1.0, 3.0) & \text{if } x < 0.5, \\ (1.0, -0.5, 2.0) & \text{if } x \geqslant 0.5. \end{cases}$$

The spatial domain is taken as $[0,1]$ with 400 mesh elements and the final time is $t = 0.5$. The solution consist of left shock, a contact and a right shock. Fig. 4 presents plots for the particle density, velocity v and pressure.

Problem 3. Perturbed relativistic shock tube flow

This problem was studied by Yang et al. [38]. The initial conditions are specified as $(n_L, u_L, p_L) = (1.0, 0.0, 1.0)$ for $0 \leqslant x \leqslant 0.5$ and $(n_R, u_R, p_R) = (n_R, 0.0, 0.1)$ for $0.5 \leqslant x \leqslant 1.0$. Here the right state is a perturbed density field of sinusoidal wave, $n_R = 0.125 - 0.0875\sin(50(x-0.5))$. We run this test for the 400 mesh points. The computed solutions are plotted at $t = 0.5$. The results for particle density n, velocity $v = u/\sqrt{1+u^2}$ and pressure p are shown in Fig. 5. Since the continuity equation in the Euler equations decouples from the other two equations for the pressure and velocity, therefore we do not see the effect of perturbation in the pressure and velocity.

Problem 4. Single shock solution of the Euler equations

In this example we test our kinetic scheme for a single shock problem. We supplied initial data to the program for which we know that a single shock solution results from the Rankine–Hugoniot jump conditions, see [24]. We select the initial data and the space–time range such that the shock exactly reaches the right lower corner at the time axis. Fig. $(6)_{1,2}$ represent the plots of the particle density in the time range $0 \leqslant t \leqslant 1.271$ and in the space range $0 \leqslant x \leqslant L = 2$. The figures shows that both first- and second-order kinetic schemes captures this shock in exactly the same way as predicted by the Rankine–Hugoniot jump conditions. The Fig. $(6)_3$ presents the particle density at the fixed time $t = 0.635$ for the same initial data. The Riemannian initial data with a jump at $x = L/2 = 1$ are chosen as

$$(n,u,p) = \begin{cases} (1.0, 0.0, 1.0) & \text{if } x < 1.0, \\ (2.725, -0.6495, 4.0) & \text{if } x \geqslant 1.0, \end{cases}$$

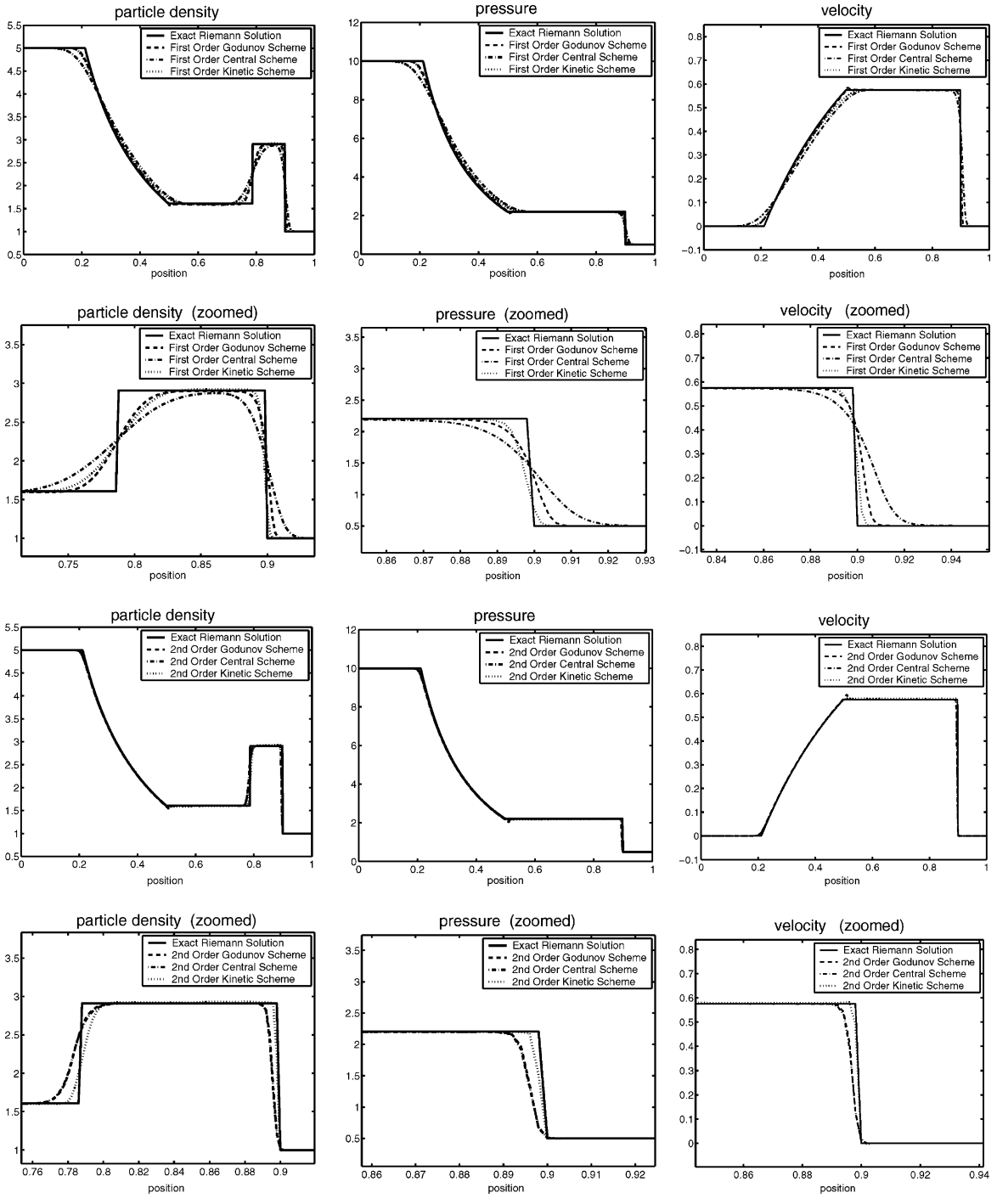

Fig. 3. Comparison of the results from the problem 1 at time $t = 0.5$.

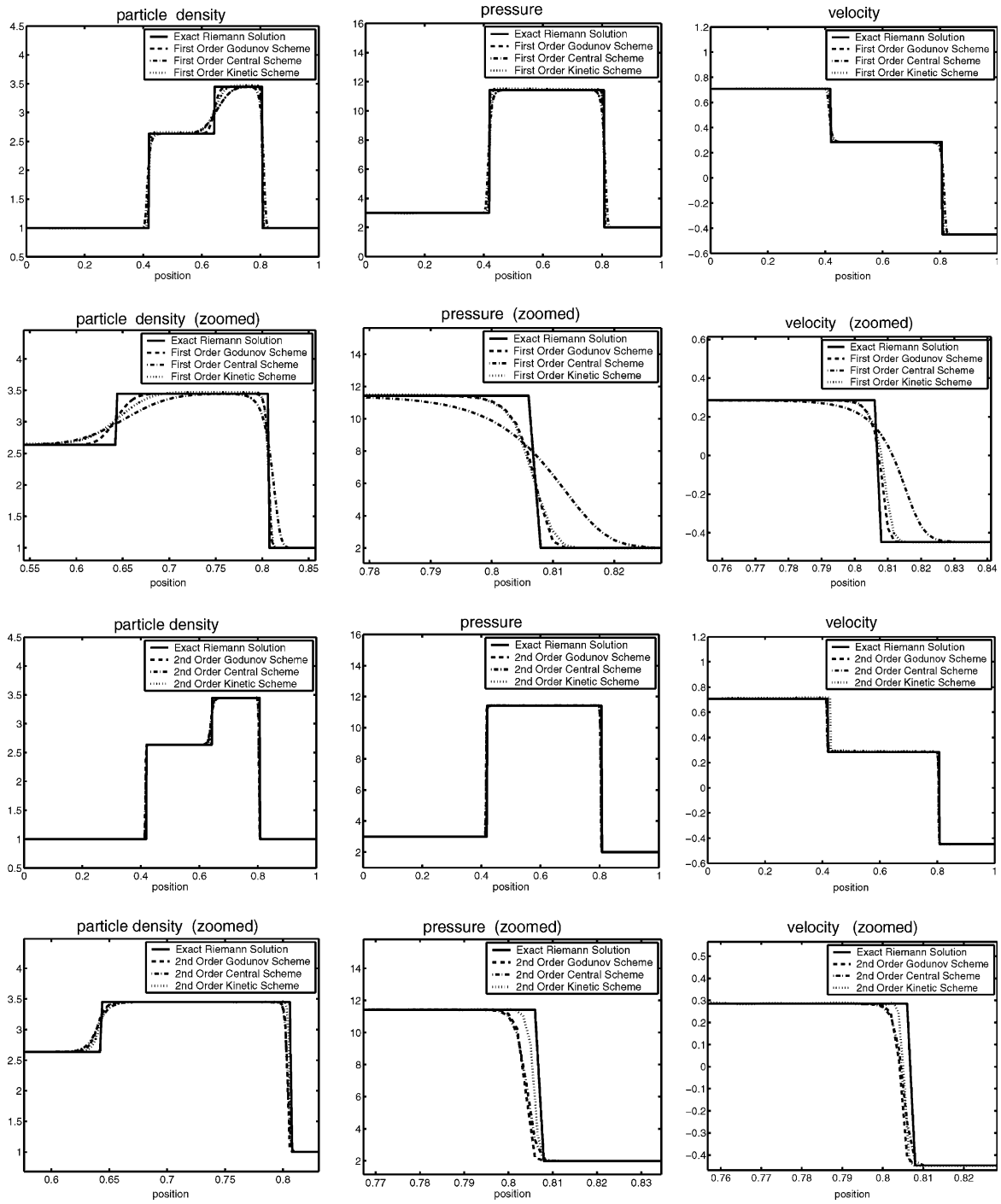

Fig. 4. Comparison of the results from the problem 2 at time $t = 0.5$.

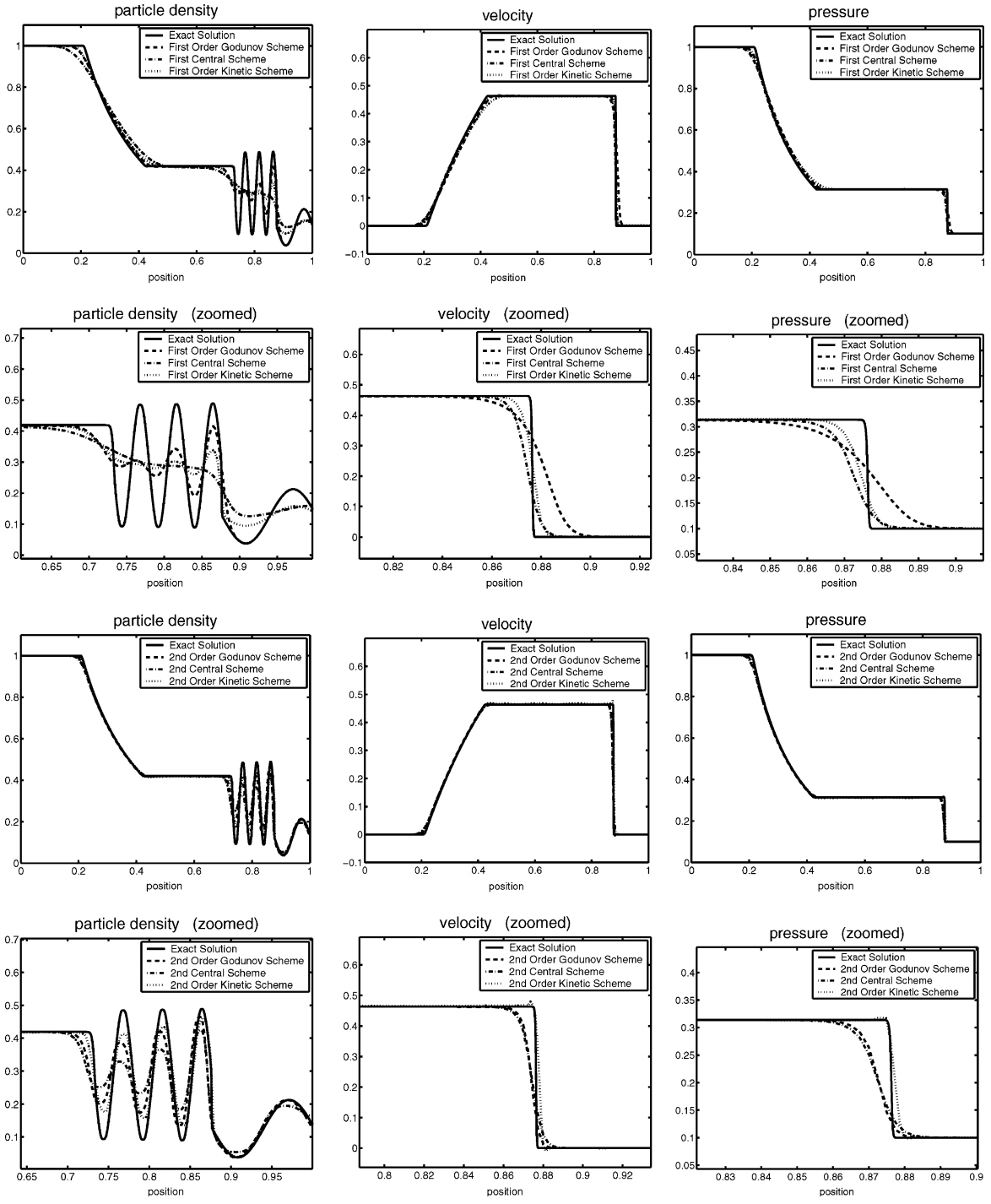

Fig. 5. Perturbed relativistic shock tube flow at time $t = 0.5$.

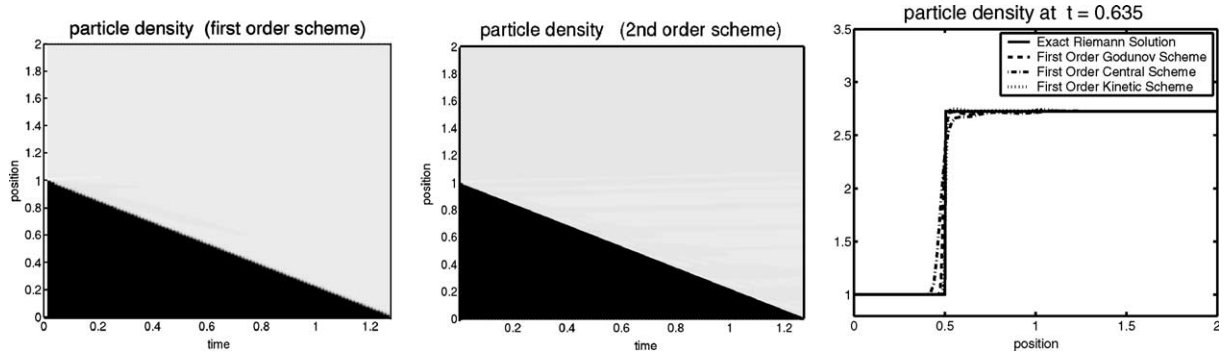

Fig. 6. A single shock solution using kinetic scheme.

where 400 mesh points are considered here. In this example we found that our kinetic scheme gives a sharp shock resolution. This is a good test for the kinetic scheme, and its success indicates that the conservation laws for mass, momentum and energy as well as the entropy inequality are satisfied, see [24].

Problem 5. Two interacting relativistic blast waves

The initial data are

$$(n,u,p) = \begin{cases} (1.0, 0.0, 100.0) & \text{if } 0 < x < 0.1, \\ (1.0, 0.0, 0.06) & \text{if } 0.1 < x < 0.9, \\ (1.0, 0.0, 10.0) & \text{if } 0.9 < x < 1.0. \end{cases}$$

The reflective boundary conditions are applied at both $x = 0.0$ and $x = 1.0$. The results are given in Fig. 7 for the particle density n, velocity v and pressure p. The number of mesh points are 1000 and the output time is $t = 0.75$.

Problem 6. From free-flight to the Eulerian limit

We consider a density distribution at zero velocity and uniform temperature:

$$n(0,x) = \begin{cases} 1, & 4.0 \leqslant x \leqslant 6.0, \\ 1.1, & \text{otherwise}, \end{cases} \quad u(0,x) = 0, \quad T(0,x) = 1.$$

We are interested in the solution within the range $x \in [0, 10]$ with 400 mesh points at time $t = 3.0$ for different maximizing entropy times τ_M. Fig. 8 depicts the density, velocity and pressure distributions at $t = 3.0$ from the first-order kinetic scheme. The diffusion like distributions result from pure free-flight with only one maximization at the beginning. The distributions that show already the formation of moving fronts are obtained when we choose $\tau_M = 0.3$, i.e. there are 10 maximizations within the time interval $[0, 3]$. When we decrease τ_M further, the fronts become steeper, and this is exhibited by the distributions that are obtained for $\tau_M = 0.03$. This is almost the Eulerian limit. The physical content of the Eulerian limit is the overwhelming importance of collisions against free-flight. A chosen $\tau_M > 0$ thus determines which of both mechanisms has more influence on a thermodynamic process. The exact Euler solution was obtained by using second-order central scheme on very fine mesh.

Problem 7. Experimental order of convergence in one space dimension

Here we check the EOC of the first and second-order kinetic schemes. The initial data are

$$n = \sin(2\pi x) + 2.0, \quad u = 0.0, \quad p = 1.0.$$

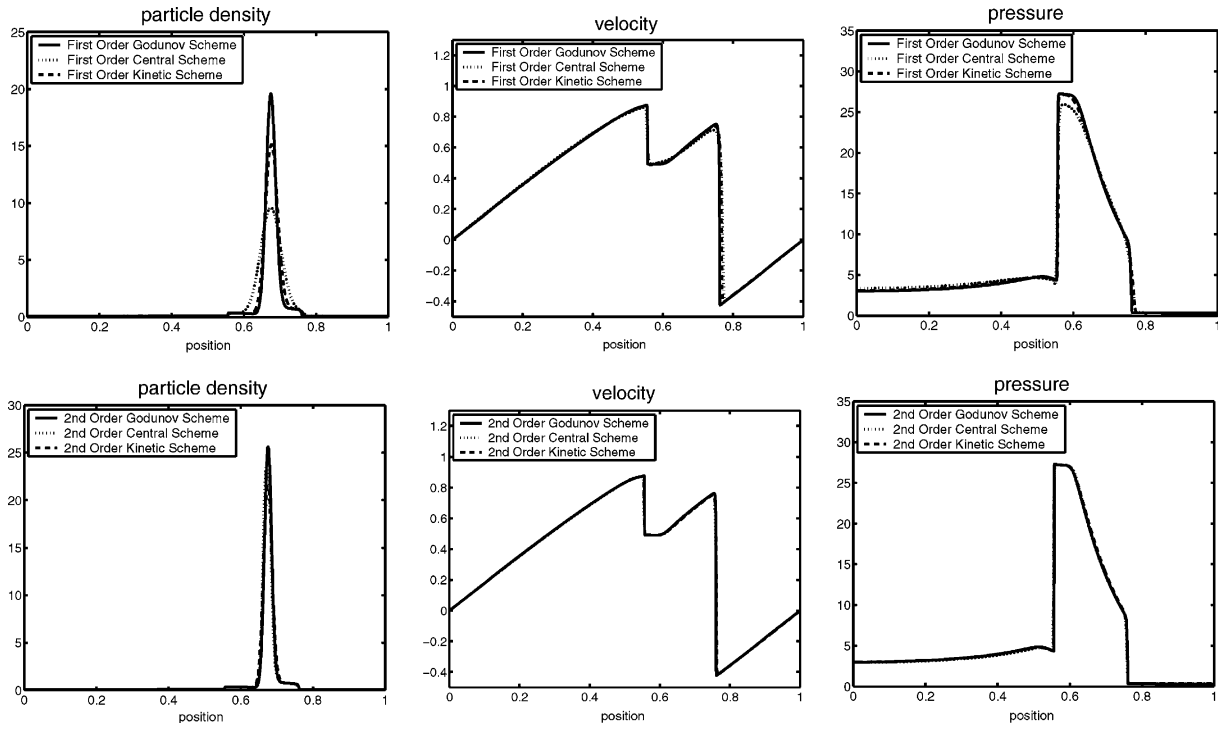

Fig. 7. Two interacting relativistic blast waves at time $t = 0.75$.

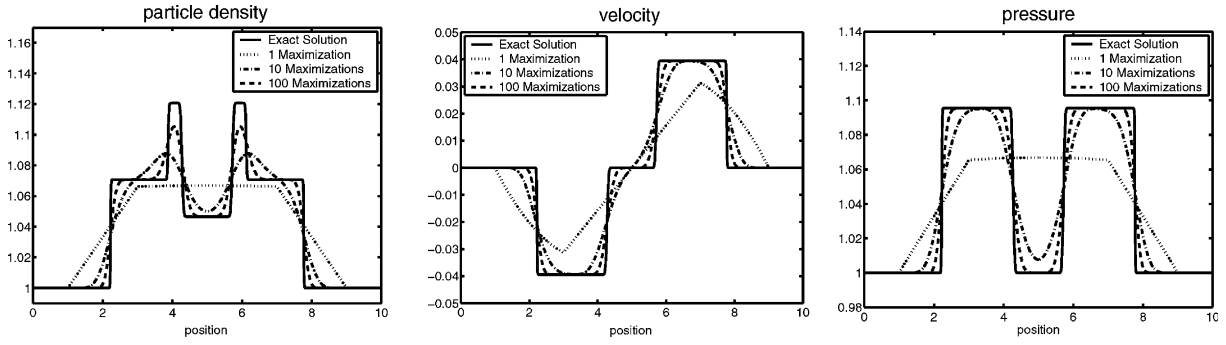

Fig. 8. Density, velocity and pressure distributions for 1, 10 and 100 maximizations.

The computational domain is $0 \leqslant x \leqslant 1$, and the final time for the numerical solution is $t = 1.0$. In a real gas there is a diffusion due to the difference in initial particle density and temperature at the initial contact discontinuity. However, this phenomenon is not described by the Euler equations. In this example the gas is initially at rest therefore the solution is stationary with same data. If $h = \Delta x$ is the cells width then L^1-norm is given by

$$\|W(\cdot,t) - W_h(\cdot,t)\|_{L^1(\mathbb{R})} = ch^\alpha, \tag{7.1}$$

Table 1
L^1-error and EOC in the kinetic scheme

N	First order		Second order	
	L^1-error	EOC	L^1-error	EOC
50	0.110296		0.012974	
100	0.057260	0.9458	0.003643	1.8324
200	0.029149	0.9741	0.001010	1.8508
400	0.014694	0.9882	0.000272	1.8927
800	0.007369	0.9957	0.000071	1.9377
1600	0.003686	0.9994	0.000018	1.9798
3200	0.001842	1.0008	4.52E − 06	1.9936

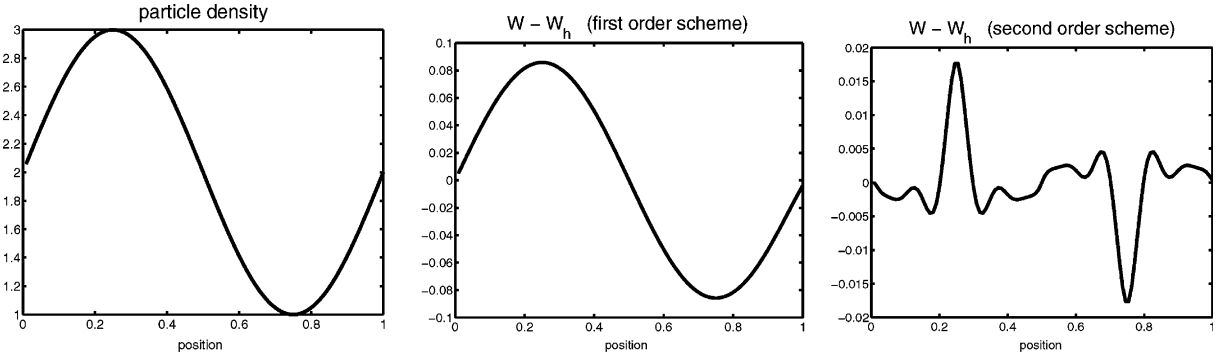

Fig. 9. Comparison of the results from the problem 6 at time $t = 0.5$.

where α is the order of the L^1-error. Here W denotes the exact solution and W_h the numerical solution. The L^1-error is defined as $\|W(\cdot,t) - W_h(\cdot,t)\|_{L^1} = \Delta x \sum_{i=1}^{N} |W(x_i,t) - W_h(x_i,t)|$, where N is the number of mesh points. Then (7.1) gives

$$\mathrm{EOC} := \alpha = \ln\left(\frac{\|W(\cdot,t) - W_{\frac{h}{2}}(\cdot,t)\|_{L^1}}{\|W(\cdot,t) - W_h(\cdot,t)\|_{L^1}}\right) \Big/ \ln\left(\frac{1}{2}\right).$$

Table 1 gives the L^1-error and EOC for the first- and second-order kinetic schemes. The plots for numerical solution and error difference in the exact and numerical solutions are given in Fig. 9.

8. Conclusions

This paper is an extension of our first-order kinetic scheme [24] to second order for the solution of ultra-relativistic Euler equations. This method is based on the well-known fact that moments of the relativistic Boltzmann equation of the kinetic theory of gases are the relativistic Euler equations when the distribution function is a relativistic Maxwellian. Thus, every method for the solution of the Boltzmann equation can be mapped to a method for the solution of the Euler equations provided the distribution function is Maxwellian. This strategy has been used to develop the kinetic scheme, which is explicit and satisfy the conservation laws and entropy inequality. Further, it can be made TVD by using a suitable interpolation strategy for evaluating the free-flight phase density. A new aspect of the present work for the relativistic case is the use of the antidiffusive Chapmann–Enskog-type distribution in developing a second-order accurate kinetic scheme. An important difference between the present kinetic scheme and other methods is the

treatment of the boundary conditions. In kinetic schemes the boundary conditions are applied on the level of distribution function which is very natural. We have numerically implemented the one-dimensional first and second-order kinetic schemes. The CFL condition for the central and Godunov schemes is very simple which is $\Delta t = \Delta x/2$. This CFL condition comes out automatically due to the structure of light cones, since every signal speed is bounded by the velocity of light. The programing codes for the kinetic schemes are simple like Godunov and central schemes. It was found that kinetic schemes give a better resolution of the contact discontinuity as compared to the Godunov and central schemes, especially in the second-order case. The kinetic scheme was found to be computationally expensive and is five to six times slower than the other schemes due to the inside loop for the **q**-integration in each computational cell. However, the kinetic schemes have other advantages. They need no CFL condition as well as are truly multi-dimensional and highly vectorizable due to their explicit nature.

Appendix A

In the following we explain the derivation of some equations used in Section 6 in order to get second-order accuracy in the one- and two-dimensional kinetic schemes for the ultra-relativistic Euler equations. In order to write the time derivatives of the fields n, u and p in term of the spatial derivatives, we use the Euler equations (3.9). These Euler equations after expanding the time and spatial derivatives gives

$$\begin{aligned}
&\sqrt{1+u^2}\frac{\partial n}{\partial t} + \frac{nu}{\sqrt{1+u^2}}\frac{\partial u}{\partial t} = -u\frac{\partial n}{\partial x} - n\frac{\partial u}{\partial x},\\
&4u\sqrt{1+u^2}\frac{\partial p}{\partial t} + 4p\frac{(1+2u^2)}{\sqrt{1+u^2}}\frac{\partial u}{\partial t} = -(1+4u^2)\frac{\partial p}{\partial x} - 8pu\frac{\partial u}{\partial x},\\
&(3+4u^2)\frac{\partial p}{\partial t} + 8pu\frac{\partial u}{\partial t} = -4u\sqrt{1+u^2}\frac{\partial p}{\partial x} - 4p\frac{(1+2u^2)}{\sqrt{1+u^2}}\frac{\partial u}{\partial x}.
\end{aligned} \tag{A.1}$$

These are three equations for three unknowns $\partial n/\partial t$, $\partial u/\partial t$ and $\partial p/\partial t$, we get

$$\begin{aligned}
&\frac{\partial u}{\partial t} = \frac{-3\sqrt{1+u^2}}{4p(3+2u^2)}\frac{\partial p}{\partial x} - \frac{-2u\sqrt{1+u^2}}{3+2u^2}\frac{\partial u}{\partial x},\\
&\frac{\partial p}{\partial t} = \frac{-2u\sqrt{1+u^2}}{3+2u^2}\frac{\partial p}{\partial x} - \frac{4p}{(3+2u^2)\sqrt{1+u^2}}\frac{\partial u}{\partial x},\\
&\frac{\partial n}{\partial t} = \frac{3n}{(3+2u^2)\sqrt{1+u^2}}\left(\frac{u}{4p}\frac{\partial p}{\partial x} - \frac{\partial u}{\partial x}\right) - \frac{u}{\sqrt{1+u^2}}\frac{\partial n}{\partial x}.
\end{aligned} \tag{A.2}$$

Using Eqs. (3.10) we can write

$$\begin{aligned}
&\frac{\partial N^1}{\partial t} = \frac{\partial}{\partial t}(nu) = u\frac{\partial n}{\partial t} + n\frac{\partial u}{\partial t},\\
&\frac{\partial T^{11}}{\partial t} = \frac{\partial}{\partial t}(p(1+4u^2)) = (1+4u^2)\frac{\partial p}{\partial t} + 8pu\frac{\partial u}{\partial t}.
\end{aligned} \tag{A.3}$$

Now using (A.2) in (A.3) we finally get after simplifications

$$\begin{aligned}
&\frac{\partial N^1}{\partial t} = -\frac{3n}{4p\sqrt{1+u^2}(3+2u^2)}\frac{\partial p}{\partial x} - \frac{(5nu+2nu^3)}{\sqrt{1+u^2}(3+2u^2)}\frac{\partial u}{\partial x} - \frac{u^2}{\sqrt{1+u^2}}\frac{\partial n}{\partial x},\\
&\frac{\partial T^{11}}{\partial t} = -\frac{8u(1+u^2)^{3/2}}{3+2u^2}\frac{\partial p}{\partial x} - \frac{4p(1+8u^2+4u^4)}{\sqrt{1+u^2}(3+2u^2)}\frac{\partial u}{\partial x}.
\end{aligned} \tag{A.4}$$

Next we want to calculate the second terms of order τ_M^2 appearing on the right-hand sides of (6.8). For this purpose we use the definitions (6.5) and reduced equilibrium phase densities (5.2), we get

$$\begin{aligned}\int_{-1}^{1}\xi^2\phi(x,\xi)\,\mathrm{d}\xi &= n\sqrt{1+u^2}\,\frac{(u^2-1)}{u^2}+\frac{n}{u^3}\ \operatorname{arcsinh}(u),\\ \int_{-1}^{1}\xi^3\psi(x,\xi)\,\mathrm{d}\xi &= \frac{p\sqrt{1+u^2}}{u^3}\left(4u^4-2u^2+3\right)+\frac{3p}{u^4}\ \operatorname{arcsinh}(-u),\end{aligned} \tag{A.5}$$

which on differentiating with respect to x gives

$$\begin{aligned}\frac{\partial}{\partial x}\int_{-1}^{1}\xi^2\phi(x,\xi)\,\mathrm{d}\xi &= \left[\frac{(u^2-1)}{u^2}\sqrt{1+u^2}+\frac{1}{u^3}\ \operatorname{arcsinh}(u)\right]\frac{\partial n}{\partial x}\\ &\quad + n\left[\frac{u^4+u^2+3}{u^3\sqrt{1+u^2}}-\frac{3}{u^4}\ \operatorname{arcsinh}(u)\right]\frac{\partial u}{\partial x},\end{aligned} \tag{A.6}$$

$$\begin{aligned}\frac{\partial}{\partial x}\int_{-1}^{1}\xi^3\psi(x,\xi)\,\mathrm{d}\xi &= \left[\frac{(4u^4-2u^2+3)}{u^3}\sqrt{1+u^2}+\frac{3}{u^4}\ \operatorname{arcsinh}(-u)\right]\frac{\partial p}{\partial x}\\ &\quad + p\left[\frac{8u^6+4u^4-4u^2-12}{u^4\sqrt{1+u^2}}-\frac{12}{u^5}\ \operatorname{arcsinh}(-u)\right]\frac{\partial u}{\partial x}.\end{aligned} \tag{A.7}$$

By using the relations (A.4), (A.6) and (A.7), we obtain after simplification

$$\begin{aligned}g(n,u,p) &= \frac{\partial N^1}{\partial t}(t_n,x)+\frac{\partial}{\partial x}\int_{-1}^{1}\xi^2\phi\,\mathrm{d}\xi\\ &= \left(-\frac{(1+u^2)^{-1/2}}{u^2}+\frac{1}{u^3}\ \operatorname{arcsinh}(u)\right)\frac{\partial n}{\partial x}-\frac{3n(1+u^2)^{-1/2}}{4p(3+2u^2)}\frac{\partial p}{\partial x}\\ &\quad +\left(\frac{9n\sqrt{1+u^2}}{u^3(3+2u^2)}-\frac{3n}{u^4}\ \operatorname{arcsinh}(u)\right)\frac{\partial u}{\partial x},\end{aligned} \tag{A.8}$$

$$h(u,p)=\frac{\partial T^{11}}{\partial t}(t_n,x)+\frac{\partial}{\partial x}\int_{-1}^{1}\xi^3\psi\,\mathrm{d}\xi=\left(\frac{9\sqrt{1+u^2}}{u^4(3+2u^2)}+\frac{3\ \operatorname{arcsinh}(-u)}{u^5}\right)\left(u\frac{\partial p}{\partial x}-4p\frac{\partial u}{\partial x}\right). \tag{A.9}$$

Eqs. (A.8) and (A.9) are appearing in the order τ_M^2 terms of $(6.8)_{1,2}$.

References

[1] P.L. Bhatnagar, E.P. Gross, M. Krook, A model for collision processes in gases, Acta Phys. Pol. 23 (1964); Phys. Rev. 94 (1954) 511.
[2] Chakravarthy, R. Sukumar, Osher, High resolution applications of the Osher upwind scheme for the Euler equations, in: Sixth AIAA Computational Fluid Dynamics Conference – Collection of Technical Papers, 1983, pp. 363–372.
[3] C. Cercignani, The Boltzmann Equation and its Applications, in: Applied Mathematical Sciences, vol. 67, Springer Verlag, New York, 1988.
[4] C. Cercignani, R. Illner, M. Pulvirenti, Mathematical Theory of Dilute Gases, in: Applied Mathematical Sciences, vol. 106, Springer Verlag, New York, 1994.
[5] N.A. Chernikov, Equilibrium distribution of the relativistic gas, Acta Phys. Pol. 26 (1964) 1069–1092.
[6] N.A. Chernikov, Microscopic foundation of relativistic hydrodynamics, Acta Phys. Pol. 27 (1964) 465–489.

[7] S.M. Deshpande, R. Raul, Kinetic theory based fluid-in-cell method for Eulerian fluid dynamics, Rep. 82 FM 14, Department of Aerospace Engineering, Indian Institute of Science, Bangalore, India, July 1982.
[8] S.M. Deshpande, A second order accurate, kinetic-theory based, method for inviscid compressible flows, NASA Langley Technical paper No. 2613, 1986.
[9] S.M. Deshpande, P.S. Kulkarni, New developments in kinetic schemes, Comput. Math. Appl. 35 (1998) 75–93.
[10] S.M. Deshpande, Kinetic flux splitting schemes, in: M. Hafez, K. Oshima (Eds.), Computational Fluid Dynamics Review 1995, John Wiley, New York, 1995.
[11] W. Dreyer, M. Kunik, Initial and boundary value problems of hyperbolic heat conduction, Cont. Mech. Thermodyn. 11.4 (1999) 227–245.
[12] C. Eckart, The thermodynamics of irreversible process I: The simple fluid, Phys. Rev. 58 (1940) 267–269.
[13] C. Eckart, The thermodynamics of irreversible process II: Fluid mixtures, Phys. Rev. 58 (1940) 269–275.
[14] C. Eckart, The thermodynamics of irreversible process III: Relativistic theory of the simple fluid, Phys. Rev. 58 (1940) 919–928.
[15] E. Godlewski, P.A. Raviart, Numerical approximation of hyperbolic systems of conservation laws, in: Applied Mathematical Sciences, vol. 118, Springer Verlag, New York, 1996.
[16] S.K. Godunov, A finite difference method for the computation of discontinuous solutions of the equations of fluid dynamics, Mat. Sb. 47 (1959) 357–393.
[17] S.R. deGroot, W.A. van Leeuven, Ch.G. van Weert, Relativistic Kinetic Theory. Principles and Applications, North-Holland, Amsterdam, 1980.
[18] A. Harten, High resolution schemes for hyperbolic conservation laws, J. Comput. Phys. 49 (1983) 357–393.
[19] A. Harten, P.D. Lax, B. Van Leer, On upstream differencing and Godunov-type schemes for hyperbolic conservation laws, SIAM Rev. 25 (1983) 35–62.
[20] W. Israel, Nonstationary irreversible thermodynamics: a causal relativistic theory, Ann. Phys. (NY) 100 (1976) 310–331.
[21] F. Jüttner, Das Maxwellsche Gesetz der Geschwindigkeitsverteilung in der Relativtheorie, Ann. Phys. (Leipzig) 34 (1911) 856–882.
[22] F. Jüttner, Die relativistische quantentheorie des idealen gases, Z. Phys. 47 (1928) 542–566.
[23] J.Mª Martí, E. Müller, Numerical hydrodynamics in speical relativity, Living Rev. Relativity 2 (1999) 1–101.
[24] M. Kunik, S. Qamar, G. Warnecke, Kinetic schemes for the ultra-relativistic Euler equations, J. Comput. Phys. 187 (2003) 572–596.
[25] M. Kunik, S. Qamar, G. Warnecke, Kinetic schemes for the relativistic gas dynamics, Preprint No. 21, Otto-von-Guericke University, 2002.
[26] M. Kunik, S. Qamar, G. Warnecke, A BGK-type kinetic flux-vector splitting schemes for the ultra-relativistic gas dynamics, Preprint No. 4, Otto-von-Guericke University, 2003.
[27] M. Kunik, S. Qamar, G. Warnecke, A reduction of the Boltzmann–Peierls equation, Preprint No. 6, Otto-von-Guericke University, 2003.
[28] H. Nessayahu, E. Tadmor, Non-oscillatory central differencing fo hyperbolic conservation laws, SIAM J. Comput. Phys. 87 (1990) 408–448.
[29] T. Ohwada, On the construction of kinetic schemes, J. Comput. Phys. 177 (2002) 156–175.
[30] O.A. Oleinik, Discontinuous solutions of nonlinear differential equations, Amer. Math. Soc. Trans. Serv. 26 (1957) 95–172.
[31] S. Osher, E. Tadmor, On the convergence of difference approximations to scalar conservation laws, Math. Comput. 50 (1988) 19–51.
[32] T. Tang, K. Xu, Gas-kinetic schemes for the compressible Euler equations: positivity-preserving analysis, Z. Angew. Math. Phys. 50 (1999) 258–281.
[33] B. van Leer, Towards the ultimate conservative difference scheme V. A second order sequel to Godunov's method, J. Comput. Phys. 32 (1979) 101–136.
[34] S. Weinberg, Gravitation and Cosmology, John Wiley, New York, 1972.
[35] K. Xu, Gas kinetic schemes for unsteady compressible flow simulations, 29th CFD, Lecture Series, 1998.
[36] K. Xu, Gas-kinetic theory based flux slitting method for ideal magnetohydrodynamics, ICASE Report No. Tr. 98-53, 1998.
[37] K. Xu, Gas evolution dynamics in Godunov-type schemes and analysis of numerical shock instability, ICASE Report No. Tr. 99-6, 1998.
[38] J.Y. Yang, M.H. Chen, I.N. Tsai, J.W. Chang, A kinetic beam scheme for relativistic gas dynamics, J. Comput. Phys. 136 (1997) 19–40.